

2

AD-A198 375

# STUDY OF HIGH TEMPERATURE FAILURE MECHANISMS IN CERAMICS

By  
Richard A. Page  
James Lankford

AFOSR FINAL REPORT

This research was sponsored by the Air Force Office of Scientific Research,  
Electronic and Materials Sciences Directorate  
Under Contract F49620-85-C-0073

Approved for release; distribution unlimited.

June 1988

DTIC  
ELECTE  
AUG 26 1988  
S H D



SOUTHWEST RESEARCH INSTITUTE  
SAN ANTONIO HOUSTON

88 3 25 1 4

SOUTHWEST RESEARCH INSTITUTE  
Post Office Drawer 28510, 6220 Culebra Road  
San Antonio, Texas 78284

# STUDY OF HIGH TEMPERATURE FAILURE MECHANISMS IN CERAMICS

By  
Richard A. Page  
James Lankford

AFOSR FINAL REPORT

This research was sponsored by the Air Force Office of Scientific Research,  
Electronic and Materials Sciences Directorate  
Under Contract F49620-85-C-0073  
Approved for release; distribution unlimited.

June 1988

Approved for public release;  
distribution unlimited.

Approved:



Gerald R. Leverant, Director  
Department of Materials Sciences

NOTICE OF TRANSMITTAL TO DTIC  
This technical report has been reviewed and is  
approved for public release IAW AFR 190-12.  
MATTHEW J. KEIRPER  
Chief, Technical Information Division

UNCLASSIFIED

SECURITY CLASSIFICATION OF THIS PAGE

ADA 198 375

REPORT DOCUMENTATION PAGE

1a. REPORT SECURITY CLASSIFICATION <b>Unclassified</b>		1b. RESTRICTIVE MARKINGS	
2a. SECURITY CLASSIFICATION AUTHORITY		3. DISTRIBUTION/AVAILABILITY OF REPORT <b>Approved for release; distribution unlimited</b>	
2b. DECLASSIFICATION/DOWNGRADING SCHEDULE			
4. PERFORMING ORGANIZATION REPORT NUMBER(S) <b>SwRI-8578/5</b>		5. MONITORING ORGANIZATION REPORT NUMBER(S) <b>AFOSR-TR. 88-0804</b>	
6a. NAME OF PERFORMING ORGANIZATION <b>Southwest Research Institute Dept. of Materials Sciences</b>	6b. OFFICE SYMBOL <i>(If applicable)</i>	7a. NAME OF MONITORING ORGANIZATION <b>Air Force Office of Scientific Research Electronic &amp; Materials Sciences Directorate</b>	
6c. ADDRESS (City, State and ZIP Code) <b>G220 Culebra Rd. (P.O. Drawer 28510) San Antonio, TX 78284</b>		7b. ADDRESS (City, State and ZIP Code) <b>Bolling AFB, Building 410 Washington, D.C. 20332</b>	
8a. NAME OF FUNDING/SPONSORING <b>AFOSR/NE Bldg 410</b>	8b. OFFICE SYMBOL	9. PROCUREMENT INSTRUMENT IDENTIFICATION NUMBER <b>F49620-85-C-0073</b>	
8c. <b>Bolling AFB, DC 20332-6448</b>		10. SOURCE OF FUNDING NOS.	
		PROGRAM ELEMENT NO. <b>61102F</b>	PROJECT NO. <b>2306</b>
		TASK NO. <b>A2</b>	WORK UNIT NO.
11. TITLE (Include Security Classification) <b>Study of High Temperature Failure Mechanisms in Ceramics (Unclassified)</b>			
12. PERSONAL AUTHOR(S) <b>Page, Richard A.; Lankford, James</b>			
13a. TYPE OF REPORT <b>Final</b>	13b. TIME COVERED <b>FROM 04/01/85 TO 03/31/88</b>	14. DATE OF REPORT (Yr., Mo., Day) <b>1988, June</b>	15. PAGE COUNT <b>66</b>
16. SUPPLEMENTARY NOTATION			
17. COSATI CODES		18. SUBJECT TERMS (Continue on reverse if necessary and identify by block number)	
FIELD	GROUP	SUB. GR.	
19. ABSTRACT (Continue on reverse if necessary and identify by block number) This report summarizes the results of a fundamental study involving experimental characterization and analytical modeling of grain boundary cavitation and creep crack growth in structural ceramics exposed to pure tensile loading. The major experimental techniques employed in the program are the use of small-angle neutron scattering to characterize cavity nucleation and growth and stereoimaging analysis to characterize the stress and strain fields associated with growing creep cracks.  The major accomplishments described in the report include the design, construction, and successful testing of a creep apparatus that permits creep testing of ceramics under pure tensile loading, the determination of surface preparation conditions that are adequate for the stereoimaging analysis, and the conduct of a series of creep tests designed to characterize the kinetics of damage accumulation under pure tensile loading. (JE)			
(continued)			
20. DISTRIBUTION/AVAILABILITY OF ABSTRACT <b>UNCLASSIFIED/UNLIMITED <input checked="" type="checkbox"/> SAME AS RPT <input type="checkbox"/> DTIC USERS <input type="checkbox"/></b>		21. ABSTRACT SECURITY CLASSIFICATION <b>Unclassified</b>	
22a. NAME OF RESPONSIBLE INDIVIDUAL <b>Dr. Alan Rosenstein Scholer</b>		22b. TELEPHONE NUMBER <b>202/767-4933</b> <i>(Include Area Code)</i>	22c. OFFICE SYMBOL <b>AFOSR/NE</b>

UNCLASSIFIED

SECURITY CLASSIFICATION OF THIS PAGE

Appended to the report is a manuscript that was prepared during the program titled, "Stochastic Aspects of Creep Cavitation in Ceramics." It is anticipated that this manuscript will provide the cornerstone for understanding creep damage and creep crack growth. Of particular interest are the development of a stochastic model of grain boundary sliding and a micromechanical model that relates the cavity nucleation rate to the statistics of grain boundary sliding events.

## TABLE OF CONTENTS

	<u>Page</u>
I. RESEARCH OBJECTIVES.....	1
II. STATUS OF THE RESEARCH EFFORT.....	2
A. Scope.....	2
B. Current Status.....	2
III. PUBLICATIONS (AFOSR SPONSORSHIP).....	9
IV. PROGRAM PERSONNEL.....	10
APPENDIX.....	A-1



Accession For	
NTIS GRA&I	<input checked="" type="checkbox"/>
DTIC TAB	<input type="checkbox"/>
Unannounced	<input type="checkbox"/>
Justification	
By	
Distribution/	
Availability Codes	
Dist	Avail and/or Special
A-1	

## I. RESEARCH OBJECTIVES

1. Utilize small-angle neutron scattering to characterize cavity nucleation and growth rates under tensile creep conditions as functions of time, temperature, stress, strain, strain rate, and microstructure.
2. Measure experimentally the local strains, grain boundary displacements, and displacement rates attendant with the above mentioned cavity characterizations.
3. Incorporate the measured cavity nucleation and growth rates and the local deformation measurements into a model for grain boundary cavitation under tensile creep.
4. Characterize creep crack growth and experimentally measure, using stereoisaging strain analysis, the crack-tip displacement field, strain singularity, and creep strain rates as functions of stress intensity, temperature, microstructure, and precavitation level.
5. Incorporate the cavitation model and measurements and the crack-tip micromechanical measurements into a fundamental creep crack growth model for ceramics.

## II. STATUS OF THE RESEARCH EFFORT

### A. Scope

Because of the attractive strength properties of ceramics at elevated temperatures, there is great interest in developing a new generation of aerospace propulsion systems capitalizing on advanced ceramics technology. These new propulsion systems would potentially offer higher operating temperatures and lower weights, thus providing dramatic increases over current engine designs in both efficiency and performance. While present engines utilize hot-stage components fabricated from nickel or cobalt-base superalloys, it is anticipated that evolving ceramic turbines will be based on silicon nitride and silicon carbide. In service, the ceramic components will experience tensile and/or cyclic loadings. Very little is known, however, about the behavior of these ceramics under tensile creep or cyclic creep conditions. An understanding of the basic failure mechanisms and an ability to predict lifetimes will be necessary before ceramics can be successfully utilized in engine applications.

In order to understand creep failure of ceramics, several specific issues must be addressed. These include: (1) characterization of the development of creep cavities at grain boundaries in bulk specimens as a function of tensile stress; (2) characterization of grain boundary displacement during bulk creep; (3) characterization of crack tip stress relaxation due to crack tip strain; (4) characterization of cavity distributions ahead of creep cracks; (5) performance of pure tensile tests at elevated temperatures; (6) creation, and characterization of the growth, of creep microcracks. The progress that has been made along these lines is summarized below. Research effort in these areas is continuing under AFOSR Contract No. F49620-88-C-0081.

### B. Current Status

Usually, "tensile" testing of ceramics has been performed in flexural bending, a compromise which produces a stress gradient across the specimen.

Pure tensile testing of brittle materials is difficult, because of alignment considerations which can produce unknown, unwanted bending moments, and hence spurious strength measurements. It is important to the goals of the proposed program to achieve pure tensile testing, however, since (1) it is desired to characterize cavitation in terms of a known applied tensile stress normal to the cavitating grain boundaries, and (2) it is necessary to secure a reasonably large sample of material cavitating at a uniform stress level for the SANS measurements. Bend tests violate both of these requirements.

A major portion of the first year of this contract was thus spent designing and fabricating a tensile creep apparatus. A schematic of the tensile creep frame is presented in Figure 1, and a close-up photograph of the environmental chamber, furnace, specimen, and gripping arrangement is presented in Figure 2. This frame utilizes deadweight loading and is capable of testing at stresses in excess of 1000 MPa and temperatures up to 2300°C. Self-aligning universal joints are affixed to the specimen grips, which, acting in conjunction with the flexures that are machined into both the upper and lower pull rods, minimize the bending moment imposed on the sample during testing.

Close-up views of the gripping assembly and specimen design are also shown in Figure 1. The grip assembly is composed of a water-cooled super-alloy main body which encloses split ceramic collets. Since ceramic specimens cannot relax plastically at grip contact points like metal alloys, boron nitride powder is used as a powder cushion lubricant between the specimen ends and the collet-type grips. The specimen design, which is based on finite element stress calculations, minimizes stress concentrations in the gage and grip areas.

Surface preparation techniques for the stereoimaging strain analysis were also examined during the first year. Generally, the stereoimaging analysis requires two photographs of the same region obtained at different deformation states; for creep loading this is accomplished by photographing the same area at various times. In this manner, the strains and strain rates can be determined. Since the analysis is a surface technique, it requires that

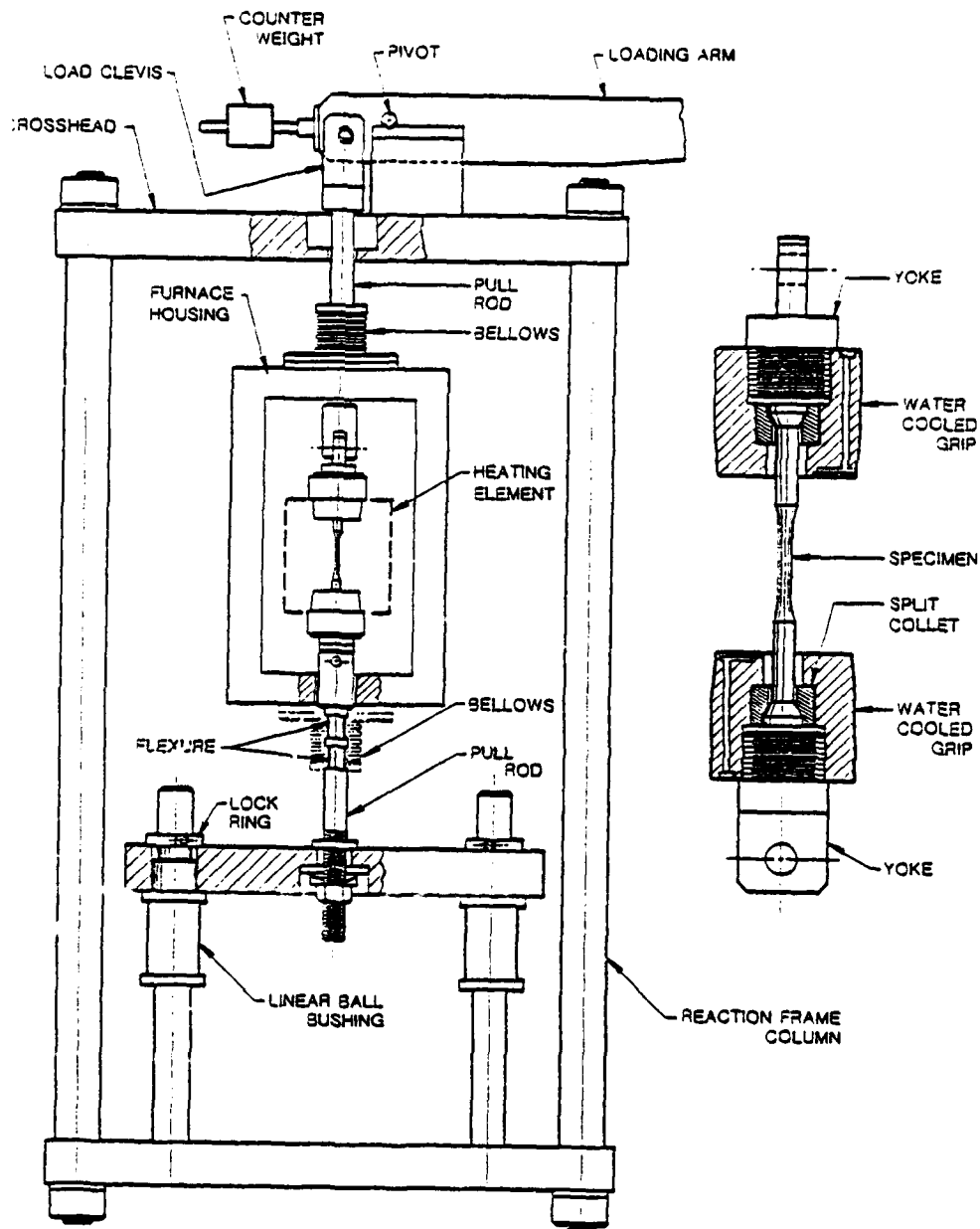


FIGURE 1. SCHEMATIC OF TENSILE CREEP FRAME. Cut-away view showing the gripping arrangement and the specimen geometry on the right.

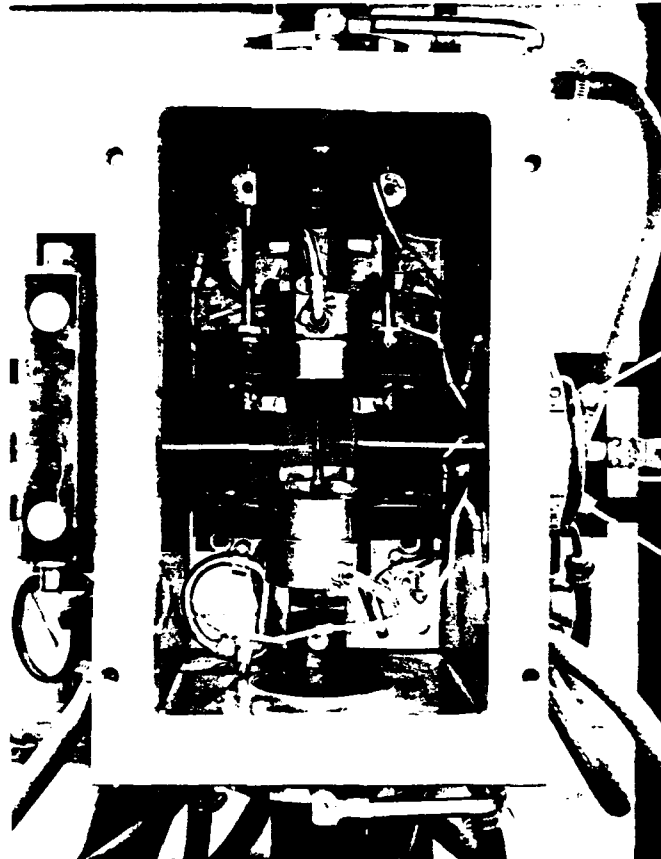


FIGURE 2. PHOTOGRAPH OF THE ENVIRONMENTAL CHAMBER OF THE TENSILE CREEP FRAME SHOWING THE FULLY ASSEMBLED GRIPPING ARRANGEMENT. Also visible are the back halves of the tungsten heating elements and the heat shields.

the surface remains unmodified, apart from modification due to the creep strains, during the time interval between the photographs. Examination of the ceramic to be used in the initial series of tests, Norton NC 203 hot-pressed silicon carbide, showed that polished surfaces were substantially modified during thermal holds at temperatures around 1600°C. Thus, as-polished surfaces are not sufficient for the stereoimaging measurements. Investigation of a number of alternate surface preparation techniques indicated that surfaces that were given a thermal etching treatment following polishing did not change dramatically during subsequent creep or thermal treatments. It thus appears that polished and thermally etched surfaces are sufficient for the stereoimaging measurements.

Effort during the second year of this contract was concentrated in three areas. The first area of effort involved problem solving in the tensile creep apparatus. The first trial runs with the system demonstrated that the specimen design was able to sustain the tensile loads required for the creep tests, the bending moment could be sufficiently minimized, and temperatures in excess of 1600°C could be reached. However, two problems were encountered; an inability to consistently reproduce the alignment conditions required to minimize the bending moment and the gradual development of oxide contamination in the furnace chamber.

To solve the former problem, the button-head and split-collect geometry were modified to permit a larger volume of boron nitride powder to be used and to allow additional freedom-of-motion for the sample during self-alignment in the boron nitride powder. Alignment checks with strain gaged specimens have shown that reproducible conditions can now be achieved. To solve the latter problem of contamination, all of the cooling water lines, which were originally a flexible nonmetallic material, were replaced with stainless steel lines. Small flexible bellows were employed at critical locations on the cooling lines to counteract the inherent rigidity of the stainless steel tubing and thus minimize any tendency of the cooling lines to impart unwanted loading to the grip assemblies.

Having corrected the alignment and contamination problems experienced in the tensile creep rig, the second area of effort involved performing a series of tensile creep experiments that form the foundation for determining cavity nucleation and growth kinetics as a function of time, temperature, stress, strain, and strain rate.

The third area of effort was the preparation of a manuscript titled "Stochastic Aspects of Creep Cavitation in Ceramics." The manuscript was published in Metallurgical Transactions, Vol. 18A, p. 1843 (1987) as an invited paper in the compendium of papers from the Stochastic Aspects of Fracture Symposium that was held at the AIME Annual Meeting in March of 1986. We anticipate that this paper will provide the cornerstone for our understanding of creep damage and creep crack growth under tensile loading. Of particular interest are the development of a stochastic model of grain boundary sliding (pp. 17-20 of the manuscript) and a micromechanical model that relates the cavity nucleation rate to the statistics of grain boundary sliding events (pp. 21-24 of the manuscript). These models have made it possible to predict the kinetics of cavity nucleation from a knowledge of the grain boundary sliding kinetics. This approach should work equally well for either bulk creep damage or localized damage around a creep crack. A copy of the manuscript has been included in the Appendix.

The shutdown of the SANS instrument at the National Center for Small-Angle Scattering Research at Oak Ridge has delayed characterization of the cavitation kinetics from the NC203 samples that were crept during the second year of the program. During this delay emphasis was redirected to the crack growth studies. High temperature creep crack growth work was initiated on a hot-pressed silicon carbide and on a pyroceram. The use of the pyroceram permits in situ crack growth studies in our high temperature SEM loading stage. Use of the scanning electron microscope (SEM) loading stage allows for real time high resolution observation of the creep crack growth process.

We have recently received a block of beam time on the SANS instrument at the Los Alamos Neutron Scattering Center. Although the Los Alamos facility is a pulsed neutron source it appears that its resolution and minimum  $q$  will

be sufficient for the required measurements. The SANS characterizations of bulk creep damage are being run concurrently with the creep crack growth studies.

### III. PUBLICATIONS (AFOSR SPONSORSHIP)

1. "Stochastic Aspects of Creep Cavitation in Ceramics," R.A. Page and K.S. Chan, Metallurgical Transactions, Vol. 18A, p. 1843, (1987).
2. "Cavitation During Tensile Creep of Silicon Carbide," R.A. Page (in preparation).

IV. PROGRAM PERSONNEL

<u>Name</u>	<u>Title</u>	
Dr. Richard A. Page	Staff Scientist	} Co-Principal Investigators
Dr. James Lankford	Institute Scientist	
Dr. Kwai S. Chan	Principal Engineer	
Mr. Andrew Nagy	Principal Engineer	
Mr. Jerry L. Sievert	Staff Technician	
Mr. Forrest S. Campbell	Staff Technician	
Mr. Arthur E. Nicholls	Senior Technician	

APPENDIX

## STOCHASTIC ASPECTS OF CREEP CAVITATION IN CERAMICS

R. A. Page and K. S. Chan  
Southwest Research Institute  
6220 Culebra Road  
San Antonio, Texas 78284

### Abstract

Creep fracture of ceramic materials frequently occurs by the nucleation, growth, and coalescence of grain boundary cavities. Recent experimental studies of cavitation kinetics in compression crept ceramics, supported by micromechanical modeling, have identified a number of stochastic aspects of cavitation. The stochastic nature of cavitation arises primarily due to the dependence of both cavity nucleation and cavity growth on grain boundary sliding. A degree of randomness is also imposed by the nonuniform distribution of potential nucleation sites. Pertinent experimental results and micromechanical models are briefly presented and used to support the important role of grain boundary sliding. A stochastic model of grain boundary sliding is then proposed by considering the sliding events to occur as an inhomogeneous Poisson process. Implications of the stochastic nature of cavitation are then discussed in terms of the cavity nucleation, growth, and coalescence processes.

## INTRODUCTION

At low or intermediate temperatures ceramic materials typically fail in a brittle manner, with the failure emanating from pre-existing flaws formed either during processing or surface finishing. Statistical models based on a weakest link approach have proven to be quite successful in predicting failure probabilities of ceramics in these temperature regimes. At elevated temperatures, however, failure of ceramic materials commonly occurs by the nucleation, growth, and coalescence of grain boundary cavities and/or microcracks (1). This increase in damage with time precludes the use of the weakest link type models. An alternative approach is, therefore, needed for predicting the failure times or probabilities of ceramic materials at elevated temperatures.

Lifetime prediction schemes based on an integration of one or more of the cavity nucleation and/or growth models have been proposed (2-5). However, although these treatments have been somewhat successful, they fail to treat the statistical aspects of cavitation. It is the purpose of this paper to establish the importance of a viable statistical failure model by demonstrating the highly stochastic nature of grain boundary cavitation and then discussing the consequences of such stochastic cavitation. Recent small-angle neutron scattering measurements of cavity nucleation and growth rates (6-10) and micromechanical models of the cavitation process (11-14) will be employed to reveal the stochastic nature of cavitation. In particular, it will be demonstrated that 1) the driving force for creep cavitation is stochastic grain boundary sliding, 2) grain boundary sliding events can be represented as an inhomogeneous Poisson process, and 3) the rate of cavity nucleation is directly proportional to

the intensity function describing the stochastic grain boundary sliding process.

Any discussion of cavitation in ceramics should give consideration to the various grain boundary microstructures available in ceramic systems and the effect that the microstructure has on the mechanisms involved in cavitation. For simplicity, only two microstructural groups will be considered in this paper; one group being composed of materials that contain no glassy second phase on the grain boundaries and the other group being composed of materials that contain a continuous glassy phase on the grain boundaries. In the following sections experimental data and micromechanical models representative of both microstructural groups will be used to illustrate the stochastic aspects of cavitation, and, despite the general consensus that the operative cavitation mechanism is different in the two microstructural groups,\* the stochastic nature of cavitation will be shown to be quite similar in both groups.

### CAVITY NUCLEATION

Cavity nucleation is most often a critical step in the creep damage accumulation process. Not only is cavity nucleation necessary to initiate intergranular fracture, but the siting of the cavities strongly affects subsequent growth and coalescence processes. Even in ceramics, which contain significant residual porosity left over from processing, cavity

---

\*Cavity growth is believed to occur by viscous hole growth when a glassy grain boundary phase is present and by grain boundary diffusion in the absence of a glassy phase.

nucleation is important. Previous studies of compressive creep in a silicon carbide with a continuous grain boundary glassy phase (8,9) and two aluminas, one with a continuous grain boundary glassy phase (9,10) and one without (6,7,9), have demonstrated that cavity nucleation definitely takes place during creep of ceramics.\* As shown in Fig. 1, cavity nucleation is frequently continuous in these systems and can be expressed in the form

$$\frac{N_c}{V} = \alpha t^\beta \quad (1)$$

where  $N_c/V$  is the number of cavities per unit volume and  $t$  is the creep time. For a given applied stress  $\alpha$  and  $\beta$  in Eq. (1) are constant. For the ceramic systems for which nucleation data has been obtained (6,7,9,10), values of  $\beta$  ranging from 0.19 to 1.0 have been obtained. These results are quite similar to the  $\beta$  values ranging from 0.38 to 1.0 that have been reported for a number of metallic materials (15-17).

The cavity densities observed in these systems are relatively high. Since there are insufficient numbers of three grain junctions to account for the majority of the cavities observed, it can be concluded that cavitation must occur on two grain facets, as well as along three grain junctions. The presence of cavities on two grain facets has been confirmed by

---

\*The small-angle neutron scattering measurements can detect cavities down to approximately 0.5-1.0 nm. This ability to detect very small cavities eliminates the possibility that the additional cavities are not nucleated but rather grow from pre-existing cavities that are below the detection limit.

direct observation with both transmission electron microscopy (7,9) and scanning electron microscopy (9,10). These observations have also shown that the cavities are predominantly present in closely spaced clusters rather than homogeneous or nearly homogeneous distributions, i.e., some facets or portions of facets are highly cavitated while other facets are completely devoid of cavitation. Additionally, the cavities in a cluster are frequently all of equal or nearly equal size, suggesting that the cavities in the cluster may have all nucleated at the same time.

Cavity nucleation in ceramics has generally been considered to occur through the clustering or condensation of vacancies on grain boundaries. Theoretical analyses indicate that stresses considerably in excess of the applied stress under which cavities are observed to nucleate are required to form a spherical cavity in materials both with (18) and without (19-21) a grain boundary glassy phase. As described in several reviews (21-26), a variety of stress concentration sites, including stress concentrations at particles, ledges, and triple points on sliding boundaries, have been proposed for reconciling the apparent discrepancy between the theoretical treatments and the experimental observations. The absence of significant numbers of grain boundary particles in the two aluminas and the silicon carbide for which cavity nucleation data is depicted in Fig. 1 rules out nucleation at particles and suggests that ledges may have been the preferred site for the nucleation of the large number of two grain facet cavities in these systems. Although information on the presence of grain boundary ledges in the silicon carbide is not yet available, high densities of ledges have been observed in aluminas with clean grain boundaries (27-29) and with continuous glassy phases (9,10). Additionally,

Wiederhorn et al (30) have observed clusters of creep cavities situated at grain boundary ledges in a glass-bonded aluminum oxide. Experimental results thus indicate that cavity nucleation is a stochastic process since it occurs at discrete points in time and space.

In order to gain a better understanding of the physical factors which may be responsible for the probabilistic nature of cavity nucleation, it is instructive to examine a relevant nucleation model. Recent work by Chan et al (14), which demonstrates that sliding along faceted grain boundaries can induce time-dependent stress concentrations of sufficient magnitude and duration to cause cavity nucleation, has been selected for this purpose since it appears to be highly relevant to the nucleation events occurring in the above mentioned ceramic systems. In the work of Chan et al (14) it was assumed that a periodic array of ledges, such as the one depicted in Fig. 2, were present on the grain boundary, and that during grain boundary sliding the boundary would lose its ability to carry shear tractions, thus converting the shear stress,  $\tau$ , into a normal stress,  $\sigma$ , concentrated at the ledges. This stress concentration would be time dependent, however, because of the gradual onset of the sliding event and the subsequent diffusive relaxation of any stress concentrations. The stress concentration at a ledge would thus be expected to initially increase, as the boundary relaxed, and then decrease, as diffusive relaxation proceeded. The time-dependent stress concentration at the grain boundary ledge,  $\sigma(x,t)$ , was found to be described by

$$\frac{\sigma(x,t)}{|\sigma_a|} = \sin\theta \cos\theta \left\{ \frac{\lambda}{h} [1 - \exp(-t/t_{BR})] \exp(-t/t_c) \exp(-2x/h) - \cot\theta \right\} \quad (2)$$

where  $\sigma_a$  is the applied stress,  $\theta$  is the angle the boundary makes with the applied stress,  $\lambda$  is the ledge spacing,  $h$  is the ledge height,  $t$  is time, and  $t_{BR}$  and  $t_c$  are the characteristic relaxation times for the relaxation of the shear stresses on the boundary and for relaxing the elastic stress concentration at the ledge by grain boundary diffusion, respectively. The solution of Eq. (2) for a ledge height of 8 nm and a ledge spacing of 400 nm along a grain boundary which is inclined at a  $45^\circ$  angle to the stress axis is illustrated in Fig. 3. It is evident from this figure that large stress concentrations can indeed develop at the ledges. However, if ledges are to act as efficient cavity nucleation sites, nucleation must occur prior to the diffusive relaxation of the stress concentration.

Chan et al (14) have calculated the characteristic times for relaxing stress concentrations at grain boundary ledges by either grain boundary diffusion or power-law creep in a pure alumina at  $1600^\circ\text{C}$  and compared them to estimates of the incubation time for cavity nucleation. The results of these calculations, Fig. 4, suggest that a narrow range of  $h/\lambda$  exists in which the incubation time for cavity nucleation is less than the characteristic time for relaxation of the stress concentration but greater than the characteristic time for relaxation of the shear tractions on the boundary. It is in this regime that cavity nucleation is expected. Another, and perhaps simpler, way of looking at the effect of the ledge height to spacing ratio is to plot the stress concentration factor, evaluated at the cavity incubation time, as a function of  $h/\lambda$ , as shown in Fig. 5. What is seen from this figure is that the stress concentration evaluated at the incubation time is small at both small and large values of  $h/\lambda$  because at small  $h/\lambda$  the shear tractions have not yet fully relaxed

and at large values of  $h/\lambda$  the stress concentration has been relaxed by grain boundary diffusion. It is only in the central regime of  $h/\lambda$  that stresses of sufficient magnitude are present for a long enough duration to result in cavity nucleation.

The above model thus suggests that cavity nucleation should be stochastic in time, due to its strong dependence on the highly stochastic process of grain boundary sliding, and also in location, due to its requirement for a specific range of  $h/\lambda$ . In other words, cavity nucleation occurs on boundaries of a particular microstructure, but only when those boundaries experience sliding.

It should be emphasized that, although the above discussion has been based on a very specific nucleation model, any nucleation mechanism that requires the development of a stress concentration at a specific microstructural feature through grain boundary sliding, as most of the mechanisms proposed to date do, would yield similar conclusions. This is likely why the stochastic nature of cavity nucleation is evident in systems with (9,10) or without grain boundary glassy phases (6,7,9) and for cavitation at triple points (31-33) or along two grain facets (6-10).

### CAVITY GROWTH

In the previous section it was shown that the dependence of cavity nucleation on grain boundary sliding imparts strong stochastic traits to the nucleation process. In this section it will be shown that grain boundary sliding may similarly affect cavity growth and thus impart unexpected transient growth behavior.

A logical starting point for the present discussion of cavity growth is a consideration of the driving force for growth. In ceramics which do not contain a glassy grain boundary phase, cavity growth is thought to occur by grain boundary diffusion, with the cavity growth rate being described by (11)

$$\dot{V} = \frac{2\pi\Omega D h (\sigma_n - 2\gamma/R)}{kT} f(\lambda/R) \quad (3)$$

where  $V$  is the cavity volume,  $t$  is time,  $\Omega$  is the atomic volume,  $D$  is the grain boundary diffusion coefficient,  $h$  is the grain boundary height,  $\sigma_n$  is the normal stress across the boundary,  $\gamma$  is the surface energy,  $R$  is the cavity radius,  $\lambda$  is the cavity spacing,  $k$  is Boltzman's constant, and  $T$  is temperature. Similarly, in ceramics which do contain a glassy grain boundary phase, cavity growth is thought to occur by a viscous process, with the cavity growth rate being described by (12)

$$\dot{R} = \frac{2/3(\lambda^2 - \beta' \pi R^2) \dot{h}}{2\pi R h \beta'} \quad (4)$$

and

$$\dot{h} = \frac{h^3 [\sigma_n - 2\gamma K (1 - 0.9\alpha'^2)]}{6\pi\lambda^2 [0.96\alpha'^2 - 1n\alpha' - 0.23\alpha'^4 - 0.72]} \quad (5)$$

where  $\alpha'$  is the ratio of the cavity radius to the cavity spacing,  $n$  is the viscosity of the glassy phase,  $\beta'$  is the cavity shape factor, and  $K$  is a constant related to the ratio of the grain boundary, surface, and interfacial energies. It is evident from the above equations that the cavity

growth rate, for either diffusive or viscous growth, is proportional to the boundary normal stress minus the sintering stress resulting from surface energy considerations. Thus, cavity growth in ceramics both with and without a grain boundary glassy phase is expected to be driven by the grain boundary normal stress in the vicinity of the cavity, with larger normal stresses resulting in more rapid growth.

Estimates of cavitation kinetics based on small-angle neutron scattering measurements of a number of different ceramics crept under compressive loading (6-10) have shown that the volume of an individual cavity can be expressed as

$$V = \alpha t^\beta \quad (6)$$

where  $t$  is the time from nucleation, and  $\alpha$  and  $\beta$  are constants. Values of  $\beta$  ranging from 0.0 to 0.62 have been obtained. Thus, previous measurements of cavity growth rates have resulted in either a zero growth rate (7,9,10), corresponding to  $\beta = 0$ , or a growth rate that decreases with time (8-10), corresponding to  $0 < \beta < 1.0$ .\* A plot of cavity radius vs time illustrating both of the above behaviors is provided in Fig. 6. It is evident from the figure that in the systems for which  $\beta$  was found to be

---

\*It is not thought that the observations of continuous cavity nucleation accompanied by limited growth are either an artifact of the measurement technique or unique to the particular systems or conditions investigated. Studies of cavitation in a number of metallic systems using techniques other than small-angle scattering have shown similar behavior (34,35).

zero, i.e., no apparent cavity growth, the constant cavity radius was considerably larger than the estimated radius of a critical cavity nucleus. Thus, a condition of  $\beta = 0$  should not be interpreted as indicating that the cavities nucleate and do not grow, but rather that a very rapid growth transient of short duration exists immediately following nucleation; the length of the transient being so short that the experimental measurements cannot detect it.

The experimental measurements presented above clearly show cavity growth in these ceramic systems as a transient, rather than a steady-state, process, and imply the existence of transient boundary tractions. The subject of transient boundary tractions, present at grain boundary ledges, was introduced in the previous section in dealing with cavity nucleation concepts. However, their extremely short duration and small spatial extent eliminate the stress concentrations formed at ledges during boundary sliding as a likely cause of the observed cavity growth transients. Two other possibilities do exist, however. Raj (36) has analyzed transient stresses arising from the nucleation of the cavities and from grain boundary sliding transients. In both cases, the characteristic relaxation time,  $t_r$  is given by (36)

$$t_r = \frac{32(1-\nu^2)L^3kT}{\pi^3EDh\Omega} \quad (7)$$

where  $\nu$  is Poisson's ratio,  $E$  is Young's modulus, and  $L$  is the characteristic diffusion length, which would be either one half of the cavity spacing for transients arising from cavity nucleation or one half of the

grain size for transients arising from the grain boundary sliding transient. The characteristic relaxation time for stress concentrations with a repeat distance equivalent to the cavity spacing ( $\sim 100$  nm) is much too short to explain the growth transients which persist for a number of hours in the silicon carbide and alumina samples for which  $0 < \beta < 1$ , although it may be of the correct duration to explain the very short transients which must occur in the systems for which  $\beta = 0$ . The characteristic time for stress concentrations with a repeat distance equivalent to the grain size is, on the other hand, of the same order as the duration of the growth transients observed when  $0 < \beta < 1$ . Hence, it appears that the cavity growth transient that one observes for  $\beta$  values between zero and one may be the result of the sliding transient that exists at the onset of grain boundary sliding.

The relationship between the grain boundary sliding rate and the driving force for cavity growth that exists during compressive creep can be seen in the viscous cavity growth model proposed by Chan et al (13). Treating the constrained growth of cavities in a material containing a continuous glassy grain boundary phase, they envisaged cavities growing on boundaries oriented parallel to the applied compressive stress in response to a local boundary normal stress that arose due to grain boundary sliding, as depicted in Fig. 7. Combining Equations (6) and (7) of Ref. (13), the average normal stress,  $\bar{\sigma}_n$ , acting on the boundary BE in Fig. 7 during steady-state sliding can be written as

$$\bar{\sigma}_n = \frac{33 \dot{U}_n}{2d} \quad (8)$$

where  $\dot{U}$  is the grain boundary sliding rate,  $\eta$  is the viscosity of the glassy phase, and  $d$  is the grain diameter. Combining Equations (4), (5) and (8) yields\*

$$\dot{R} = \frac{h^2(2\sqrt{3}k^2 - \beta' \pi R^2) \left[ \frac{33 \dot{U} \eta}{2d} - 2\gamma K(1 - 0.9\alpha'^2) \right]}{12\pi R \beta' \eta k^2 [0.96\alpha'^2 - \ln\alpha' - 0.23\alpha'^4 - 0.72]} \quad (9)$$

When viewed in this manner, it is clear that the grain boundary sliding rate provides the driving force for cavity growth during compressive creep. If one considers only steady-state sliding, then the growth behavior depicted by the dashed line in Fig. 8 is predicted by Equation (9). There is good agreement between theory and experiment in the steady state region. On the other hand, the constrained growth model (13), from which Equation (9) was derived, does not do an adequate job of modeling the time dependence of the experimentally measured growth rate in the transient region; leading, once again, to the conclusion that stress transients arising from sliding transients must be considered for the observed growth transients. In addition to its important role in cavity nucleation, the stochastic process of grain boundary sliding, thus, appears to play a significant role in cavity growth during compressive loading as well. Disregard for the stochastic aspects can lead to large errors in cavity growth rate predictions.

---

\*Although not presented here, a similar treatment can be performed with Eq. (3) for cavity growth on clean grain boundaries.

Caution must be employed when trying to apply the above arguments, which were derived for compressive loading, to cavity growth under tensile loading. In a compressive creep test, most if not all of the normal stress on the cavitating tensile boundaries arises through grain boundary sliding. On the other hand, grain boundary sliding and the applied tensile stress both contribute to the normal tractions during tensile creep. Thus, although sliding transients are expected under tensile loading, they may not dominate the cavity growth process in tension as they apparently do in compression. The effect of the sliding transients on cavity growth during tensile creep would, of course, depend on the relative magnitudes of the normal tractions developed through sliding and directly through tensile loading. A series of creep cavitation experiments are presently in progress to characterize cavitation kinetics under uniaxial tensile loading.

#### DEFORMATION CHARACTERISTICS IN CAVITATION OF CERAMICS

The preceding review indicates the important role of grain boundary sliding in the cavitation process of ceramics at elevated temperatures. Specifically, grain boundary sliding provides the driving force for cavity nucleation and/or growth in ceramics by inducing a local, transient tensile stress at grain boundary ledges (7,14), particles (3,36,37), or triple-points (38,39). Both the applied stress and the sliding-induced tensile stress contribute to the driving force for cavitation in ceramics under remote tension, while for ceramics under compressive loading, the sliding-induced local tensile stress represents the sole source of the

driving force for cavitation. Previous reviews (40,41) indicated that, in both ceramics and metals, the contribution of grain boundary sliding to the macroscopic creep rate can be substantial. In many instances, the grain boundary sliding displacement was found to be discontinuous with time (41), indicating the stochastic nature of the process. As alluded to earlier, stochastic grain boundary sliding accounts for the observations of: 1) continuous cavity nucleation in ceramics with clean boundaries (6,7) as well as in ceramics with grain boundary amorphous phases (9,10), and 2) transient cavity growth in ceramics with glassy phases along grain boundaries (8-10).

For compatibility reasons, grain boundary sliding in polycrystalline materials is restricted or constrained in the sense that the displacement of a sliding boundary must be accommodated by the neighboring grains (37). As a result, sliding-induced cavity nucleation and growth occur in a constrained manner and, because of the need for accommodation, is often controlled by diffusion and/or the deformation characteristics of the matrix (42), depending on the accommodation process which can be diffusive and/or dislocation creep. The role of grain deformation characteristics in constrained cavity nucleation and/or growth can be elucidated by considering the contribution of individual grains to the macroscopic strain rate in a polycrystalline material containing grains which deform initially at  $t < t_1$  at a constant creep rate,  $\dot{\gamma}_c$ , and a constant sliding rate,  $\dot{\gamma}_s$ . The total, macroscopic shear strain rate,  $\dot{\gamma}_t$ , equals the sum of  $\dot{\gamma}_s$  and  $\dot{\gamma}_c$ . Defining  $\dot{\gamma}_s/\dot{\gamma}_t$  as  $\lambda$ , the probability density function for grains of a given value of  $\lambda$  is then represented by the delta function, as illustrated in Fig. 9. At  $t > t_1$ , stochastic grain boundary sliding is allowed to occur

in some of the grains such that  $V_i$  represents the volume fraction of the  $i$ th group of grains creeping at  $\dot{\gamma}_C^i$  and sliding at  $\dot{\gamma}_S^i$ . Under this circumstance,

$$\dot{\gamma}_t = \sum_{i=1}^{\mathcal{L}} V_i (\dot{\gamma}_S^i + \dot{\gamma}_C^i) \quad (10)$$

with  $\mathcal{L}$  being the total number of groups of grains deforming and creeping at different values of  $\Lambda^i$  ( $\Lambda^i = \dot{\gamma}_S^i / \dot{\gamma}_t$ ). For constrained deformation,

$$\dot{\gamma}_t = \dot{\gamma}_S^i + \dot{\gamma}_C^i \quad (11)$$

for all values of  $\Lambda^i$  ranging from 0 to 1. Substituting Eq. (11) into Eq. (10) leads to  $\sum V_i = 1$ , as it should. The probability density function for grains of a given value of  $\Lambda^i$  is, however, no longer described by the delta function but instead by one which shows a finite probability value for each possible value of  $\Lambda^i$  (Fig. 9). Thus, the volume fraction of grains sliding at a given  $\Lambda^i$  ratio varies with time, even though the macroscopic strain rate,  $\dot{\gamma}_t$ , is constant for constrained deformation. A relevant stochastic grain boundary sliding model must therefore consider the number of grain boundary sliding events or grains with time.

The largest grain boundary sliding rate would, of course, be associated with grains with a large  $\Lambda$  value (e.g.,  $\Lambda = 1$ ). As grain boundary sliding provides the driving force for cavitation, grains with large  $\Lambda$  values would be the most likely regions where cavity nucleation and/or

growth would occur. The initial population of these grains in a polycrystalline ceramic is probably small, as illustrated in Fig. 9. Consequently, grains with large sliding components (large  $\Delta$ ) are likely to be surrounded by grains of large creep components (small  $\Delta$ ). The ramification is that in a polycrystalline ceramic some grain boundaries are susceptible to cavitation while adjacent boundaries might not be. Cavitation would therefore occur in clusters, as observed experimentally (7). In addition to the presence of grain boundary sliding, the cavitation susceptibility of a grain boundary increases with the presence of ledges and/or particles and varies with grain size and surface energy. Hence, a nonuniform distribution of ledges, particles, grain size, and surface energy among individual grain boundaries would also lead to heterogeneous cavitation.

#### STOCHASTIC MODELING OF GRAIN BOUNDARY SLIDING

Stochastic grain boundary sliding was experimentally observed in Cu (43), Al (44-47), and Sn (48) bicrystals; these earlier works were thoroughly reviewed in Ref. 49. In the study on Cu bicrystals, Intrater and Machlin (43) found that each of the stochastic grain boundary sliding events was distinct with the sliding distance/time curves being characterized by null displacement periods and sudden displacement jumps. These characteristics suggest that stochastic grain boundary sliding satisfies the four assumptions for a point process (50): (i) all epochs of the grain boundary sliding events are distinct, (ii) any finite time interval contains only a finite number of epochs, (iii) any infinite time interval contains an infinite number of epochs, and (iv) grain boundary sliding

events do not occur at predetermined times. For sliding under constrained conditions, the grain boundary sliding process can be considered to evolve without aftereffects, i.e., the past sliding behavior has no influence on the future behavior (50). Under this circumstance, the counting process,  $N(t)$ , associated with grain boundary sliding can be represented as an ordinary continuous time stochastic process with the number of sliding events with epochs in the time intervals  $(t_1, t_2]$  described by the Poisson distribution. The probability law of the stochastic sliding process is then completely specified by its mean function (50).

The mean function,  $\mu'(t)$ , is the expected value of  $N(t)$  of the point process, i.e.,  $\mu'(t) = E[N(t)]$ ,  $t \geq 0$ , in which  $\mu'(t)$  represents the mean value of the number of grain boundary sliding events at time  $t$ . Since  $N(0) = 0$  and  $N(t)$  approaches infinity as time approaches infinity (Condition iii), it follows that (50)

$$\mu'(t) = 0 \quad \text{for } t = 0 \quad (12)$$

and

$$\mu'(t) \rightarrow \infty \quad \text{as } t \rightarrow \infty. \quad (13)$$

In addition, the mean function must be a strictly increasing function of time as

$$d\mu'(t) \triangleq \mu'(t + dt) - \mu'(t) = E[N(t + dt) - N(t)] \quad (14)$$

is the expected number of grain boundary sliding events in  $(t, t + dt)$  and it is always positive. In general, the mean function  $\mu'(t)$  can be represented by the integral (50)

$$\mu'(t) = \int_0^t \lambda'(t) dt \quad t \geq 0 \quad (15)$$

where  $\lambda'(t)$  is the intensity function of the point (grain boundary sliding) process. Combining Equations (14) and (15) leads to

$$\lambda'(t) \equiv \frac{d\mu'(t)}{dt} > 0 \quad (16)$$

which indicates that the intensity function,  $\lambda'(t)$ , must be a positive constant (homogeneous Poisson process) or a positive function of time (inhomogeneous Poisson process) for all time.

A simple function that can be used for describing the mean value of the number of grain boundary sliding events at time  $t$  is\*

$$\mu'(t) = \frac{a_0}{1-m} t^{1-m} \quad (17)$$

with

$$\lambda'(t) = a_0 t^{-m} \quad (18)$$

---

\*Other simple functions such as  $\ln t$ ,  $e^t$ , and  $e^{-1/t}$  have been considered but none of them are admissible in a Poisson process.

where  $a_0$  and  $m$  are constants. Equations with forms similar to Eqs. (17) and (18) have been used previously for modeling stochastic cavity nucleation (51). To satisfy the conditions specified in Eqs. (12) (13) and (16) for a Poisson process,  $a_0$  must be greater than zero ( $a_0 > 0$ ) and  $m$  must be less than unity ( $m < 1$ ). If the average sliding distance for a sliding event is  $\langle x \rangle$ , the total grain boundary sliding rate,  $\dot{U}$ , then becomes

$$\dot{U}(t) = \langle x \rangle \lambda'(t) = a_0 \langle x \rangle t^{-m} \quad (19)$$

leading to

$$U(t) = \frac{a_0 \langle x \rangle}{1-m} t^{1-m} \quad (20)$$

the functional behavior of which is illustrated in Fig. 10 for three different limits of  $m$  values. A review of the grain boundary sliding measurements compiled in Ref. 49 indicates that the experimental sliding/time curves are described by Eq. (20) with  $0 < m < 1$ . It can thus be concluded that stochastic grain boundary sliding can be modeled as an inhomogeneous Poisson process with an intensity function,  $\lambda'(t)$ , decreasing with time. Both Eqs. (17) and (18) have been used for developing a stochastic cavity nucleation model (in the following section) and a cavity coalescence model (52).

## IMPLICATIONS ON CAVITATION MECHANISMS OF CERAMICS

The conventional view of cavitation in ceramics is that it proceeds by void nucleation, growth, and coalescence mechanisms. Cavities are presumed to nucleate primarily near three-grain junctions (triple points), and then propagate along grain facets to form facet-sized cavities (31). The facet-sized cavities are then stabilized; coalescence occurs when facet-sized cavities form on continuous boundaries. While this particular cavitation mechanism has been observed (39), there is increasing experimental evidence, obtained based on transmission electron microscopy (14,30) and small-angle neutron scattering measurements (6-10), which indicates that creep cavities in ceramics nucleate at ledges along two-grain junctions. This observation has been observed in ceramics both with (8-10,30) and without (6,7,14) grain boundary amorphous phases.

Nucleation of cavities at grain boundary ledges requires a high local tensile stress which can be achieved only at grain boundary ledges within a certain range of height/spacing ratios (14). The height/spacing limitation exists because: 1) the stress concentration at the ledges is relaxed by grain boundary diffusion, the effectiveness of which depends on the ledge spacing, and 2) the stress concentration must persist over a time period longer than that of the incubation time for cavity nucleation. The consequence is that only grain boundaries containing ledges which satisfy the height/spacing requirement are possible nucleation sites. Sliding of grain boundaries containing ledges which do not satisfy the ledge height/spacing requirement would not be expected to nucleate cavities until additional ledges are introduced, possibly by the intersection of slip with the grain boundaries, such that the necessary ledge

height/spacing ratio is met. Thus, continuous cavity nucleation requires grain boundary sliding and possibly the generation of slip steps along the grain boundaries, both of which are stochastic processes.

If one considers thermal nucleation, the rate of cavity nucleation is given by (3,36,38)

$$\dot{n} = C n_0 \quad (21)$$

with 
$$C = \frac{C'}{\sigma} \exp(-4\gamma^3 F_v / \sigma^2 kT) \quad (22)$$

where  $n_0$  is the number of available nucleation sites per unit area of grain boundary,  $C'$  is a constant, and  $F_v$  is the cavity shape parameter which yields the volume of the cavity when multiplied by  $R^3$ . The cavity nucleation rate is generally dominated by the exponential term in Eq. (22). The importance of the large transient normal stress induced at grain boundary ledges or particles by stochastic grain boundary sliding is therefore quite obvious. Additionally, the cavity nucleation rate also depends on  $n_0$  which in turn is dependent on the number of grain boundary sliding events. In the time interval  $(t, t+\epsilon]$ ,

$$n_0 = \lambda'(t)\epsilon r \quad (23)$$

where  $\epsilon$  is the time period within which the large transient stress due to grain boundary sliding exists (see Fig. 3),  $r$  is the number of eligible nucleation sites (with proper  $h/\lambda$  for nucleation at ledges (14) or proper particle size to spacing ratios for nucleation at particles (53)) per unit

area of an individual sliding boundary, and  $\lambda'(t) = du'(t)/dt$  represents the rate of increase of the number of sliding events. Combining Eqs. (18) and (23) with Eq. (21) leads to

$$\dot{n} = C_0 a_0 t^{-m} \quad (24)$$

where  $C_0 = C_\epsilon r$  is a constant which depends on temperature but not on time, assuming the number of eligible nucleation sites ( $r$ ) per unit area of an individual sliding boundary does not significantly vary with time. Integration of Eq. (24) results in

$$\frac{N_c}{V} = \frac{C_0 a_0}{1-m} t^{1-m} \quad (25)$$

or

$$\frac{N_c}{V} = C_0 \mu'(t) \quad (26)$$

which relates the number of cavities directly to the number of stochastic grain sliding events. The time dependence of  $\dot{n}$  and  $N_c/V$  for permissible values of  $m$  are illustrated in Fig. 10. Comparing Eq. (1) with Eq. (25) reveals that  $\beta = 1-m$ . Since  $0 < m < 1$  for stochastic grain boundary sliding, the value of  $\beta$  would also range from zero to unity ( $0 < \beta < 1$ ) as observed experimentally for many metals (15-17) and ceramics (6,7,9,10). To the authors' knowledge, there are no measurements of grain boundary sliding and cavity nucleation that have been performed on the same metallic or ceramic system available in the literature. As a result, it is not possible at the present time to verify the model prediction that the same

time exponents (i.e., the same value of  $m$ ) occur in Eqs. (20) and (25), nor the assumption that  $r$  remains constant with time.

A direct consequence of the intimate relationship between stochastic sliding and cavity nucleation is that the initial growth of sliding-induced cavities is inherently transient. For cavity growth to continue, the sliding-induced local tensile stress must not diminish, as a consequence of diffusive or viscous relaxation, at a rate faster than that of the sintering stress. When sufficient tensile stress is maintained, the cavities would grow and ultimately coalesce to form a grain facet cavity or crack, Fig. 11. On the other hand, sintering occurs when the local tensile stress diminishes faster than the sintering stress. For ceramics which show zero apparent cavity growth rate, the local tensile stress is exactly balanced by the sintering stress. Under this circumstance, cavitation proceeds by nucleating new cavities at regions adjacent to the existing cavities. The joining of these cavities eventually leads to a grain facet cavity (Fig. 12).

A question that has not been completely resolved is what is the preferred orientation, if any, for grain boundary cavitation (54,55). The general belief is that grain boundary sliding is required to provide the stress concentration for cavity nucleation; the nucleation rate is therefore expected to peak at inclined boundaries where sliding is a maximum. On the other hand, the preferred locations for either diffusive or viscous cavity growth would be boundaries that are inclined at  $90^\circ$  and  $0^\circ$  to the stress axis when under tension and compression, respectively. A different

view was offered by Chen (54) who argued that grain boundary sliding is mainly the consequence of requiring compatibility among grains in a polycrystal, and that the magnitude of sliding has little correlation with the resolved shear stress that is present on the grain boundary before relaxation occurs. Citing the earlier work of Mullendore and Grant (56), and Fazan et al (57), Chen suggested that grain boundary sliding is statistically independent of the boundary inclination with respect to the applied stress axis. If sliding is indeed independent of boundary angle, then, for materials under tension, the factor which influences cavitation is the normal component of the applied stress whether or not the growth mechanism is assisted by grain boundary sliding. Recent work (55,58) has indicated that most of the cavitated boundaries in either metals or ceramics are normal to the stress axis when under tension (7,55,58), but are parallel to the stress axis when under compression (7).

#### IMPLICATIONS ON COALESCENCE OF FACET-SIZED CAVITIES

The mechanisms which lead to final failure of ceramics are: 1) coalescence of facet-sized cavities to form a macrocrack, and 2) the propagation of the macrocrack to a critical size (31). As indicated earlier, there are preferred boundaries for cavity nucleation and growth because the number of sliding events and the cumulative grain boundary sliding distance differ among grains. In addition, there are also variations in the grain size, surface energy, ledge height and spacing, and particle distribution. Thus, coalescence of facet-sized cavities needs to be treated as a stochastic process and analyzed by statistical means.

The mechanisms by which facet-sized cavities coalesce are different in ceramics under tension and compression. As illustrated in Fig. 13(a), coalescence of facet-sized cavities under tension proceeds in a manner which leads to a macroscopic crack that lies normal to the applied stress axis (31), i.e., a Mode I crack. The criticality of such a crack can be expressed in terms of a critical  $K_c$  value. On the other hand, in ceramics under compression, a majority of the facet-sized cavities lie parallel to the compressive stress axis and coalescence of these facet-sized cavities occurs by a shear process (59), Fig. 13(b).

A statistical model which describes coalescence of facet-sized cavities under tension is that of Evans and Rana (31). In this model, the cumulative probability of observing facet-sized cavities is assumed to be a Weibull distribution (60) expressed in terms of the time,  $t_p$ , required for a cavity to nucleate at a triple point and propagate along the two grain channel until a facet-sized cavity is formed. The coalescence of the facet-sized cavities to form a macroscopic crack of a given size is then represented by the probability function due to McClintock (61) by assuming that there is no interaction between individual facet-sized cavities. For ceramics under nominally elastic, tensile loading, Evans and Rana's model (31) leads to a creep-rupture criterion which relates the Orr-Sherby-Dorn rupture parameter (62) to the remotely applied stress, fracture toughness, and the propagation time,  $t_p$ , for a particular cavity growth process. Good correlations have been obtained between the proposed rupture criterion and rupture life data of  $Al_2O_3$  and SiC fibers (31).

One advantage of the Evans and Rana statistical model (31) is that it can be easily adapted to different cavity growth mechanisms by modifying the propagation time,  $t_p$ . On the other hand,  $t_p$  does not describe the driving force for cavitation, but is rather the response of the material subjected to such a driving force. From previous discussion, it is clear that grain boundary sliding represents, at least partially if not totally, the driving force for cavitation. It would, therefore, seem more appropriate to describe the coalescence of facet-sized cavities on the basis of the grain boundary sliding displacement or the sliding events.

A model which describes coalescence of facet-sized cavities in terms of stochastic grain boundary sliding does not exist at the present time, however. A possible approach for modeling the coalescence of facet-sized cavities is to represent the cumulative probability,  $F(U_s)$ , of observing facet-sized cavities at a grain boundary sliding distance  $U_s$  in terms of a three-parameter Weibull distribution:

$$F(U_s) = 1 - \exp \left[ - \left( \frac{U_s - U_{th}}{U_0} \right)^r \right] \quad (27)$$

where  $r$  is the shape parameter,  $U_0$  is the scale parameter, and  $U_{th}$  is the threshold distance which grain boundary sliding must exceed in order to produce cavity nucleation and/or growth. The number of facet-sized cavities,  $N$ , at a sliding distance of  $U_s$  is then given by

$$N = n_b n_g P_s \left\{ 1 - \exp \left[ - \left( \frac{U_s - U_{th}}{U_0} \right)^r \right] \right\} \quad (28)$$

where  $n_b$  is the number of grain boundary facets per grain,  $n_g$  is the number of grains, and  $P_s$  is the probability of the grain containing boundaries that would slide. For  $U_s - U_{th} < U_0$ , Eq. (28) can be approximated as:

$$N = \phi_s P_s \left( \frac{U_s - U_{th}}{U_0} \right)^r \quad (29)$$

in which the parameter,  $\phi_s (= n_b n_g)$ , describes the shape and density of grains within a particular volume,  $V$ , of material. For cuboidal grains of average size  $d$ ,

$$\phi_s = \frac{6V}{d^3} \quad (30)$$

and

$$\phi_s = \frac{84V}{\pi d^3} \quad (31)$$

for tetrakaidecahedral grains when the volume of a tetrakaidecahedron is approximated as  $\pi d^3/6$ . The probability that a particular grain would experience grain boundary sliding and cause cavitation can be approximated by the volume fraction,  $V_s$ , of grains with  $\lambda \approx 1$  (recalling  $\lambda = \dot{\gamma}_s / \dot{\gamma}_t$ ). Eq. (29) thus becomes

$$N = \phi_s V_s \left( \frac{U_s - U_{th}}{U_0} \right)^r \quad (32)$$

which can be differentiated with respect to time to obtain the rate of formation of facet-sized cavities, yielding

$$\dot{N}_V = N_V \left[ \frac{\dot{V}_S}{V_S} + \frac{r\dot{U}_S}{U_S - U_{th}} \right] \quad (33)$$

where  $N_V$  is the facet-sized cavity density. Equation (33) indicates that the facet-sized cavity nucleation rate,  $\dot{N}_V$ , can be fully described in terms of the current facet-sized cavity density, the sliding displacement rate, and the rate of change of the volume fraction of grains that manifest grain boundary sliding. Thus, both  $\dot{V}_S$  and  $\dot{U}_S$  must be considered when modeling the coalescence of facet-sized cavities. Efforts to develop such a cavity coalescence model are currently being undertaken by the authors and the results are to be presented shortly (52).

In addition to a statistical description of the formation of facet-sized cavities, statistical representations of the cavity nucleation and/or growth processes that lead to the facet-sized cavities are also needed to completely describe cavitation in ceramics and to predict time to failure. These statistical analyses would need to consider the following stochastic processes: 1) ledge formation along two-grain junctions; 2) nucleation of cavities at the grain boundary ledges; 3) coalescence of cavities located at two-grain junctions by either cavity growth or the nucleation of additional cavities. In the analysis of cavity growth, the effect of nonperiodic spacing might also be considered. Recent Monte-Carlo simulations indicate that the time to rupture is affected by the periodicity of the cavities (63) and also depends on whether cavities are allowed to nucleate at regions adjacent to the existing cavities (51).

### SUMMARY

A number of stochastic aspects of creep cavitation in ceramics have been identified. This stochastic nature originates primarily from the dependence of both cavity nucleation and cavity growth on the highly stochastic process of grain boundary sliding. A degree of randomness is also imposed by the nonuniform distribution of nucleation sites dictated by the narrow range of  $h/\lambda$  for which nucleation is likely to occur. In addition to the effect on cavity nucleation and growth, the time and spatial discreteness of cavitation also influences the critical process of cavity coalescence. Statistical models are therefore needed for accurate life-time predictions in these materials. Such models may be based either on the perceived response of the material or on the driving force for cavitation. A stochastic model is proposed for grain boundary sliding and used for predicting cavity nucleation. Important findings of the modeling effort are: 1) the relevant driving force for creep cavitation is stochastic grain boundary sliding, 2) stochastic grain boundary sliding is an inhomogeneous Poisson process, and 3) the cavity nucleation rate is directly proportional to the intensity function while the number of cavities/volume is directly proportional to the mean function describing the stochastic grain boundary sliding process. Presently, life prediction attempts are limited by a lack of statistical representations of the cavity nucleation and/or growth processes that lead to the formation of facet-sized cavities.

**ACKNOWLEDGEMENT**

The preparation of this manuscript was supported by the Air Force Office of Scientific Research under Contract F49620-85-C-0073.

## REFERENCES

1. A. G. Evans: Recent Advances in Creep and Fracture of Engineering Materials and Structures, B. Wilshire and D. R. J. Owen, eds., Pineridge Press, Swansea, U.K., 1982, pp. 53-133.
2. D. Hull and D. E. Rimmer: Phil. Mag., 1959, vol. 4, pp. 673-689.
3. R. Raj and M. F. Ashby: Acta Metall., 1975, vol. 23, pp. 653-666.
4. A. C. F. Cocks: Acta Metall., 1985, vol. 33, pp. 129-137.
5. P. M. Anderson and J. R. Rice: Acta Metall., 1985, vol. 33, pp. 409-422.
6. R. A. Page and J. Lankford: J. Am. Ceram. Soc., 1983, vol. 66, pp. C-146-148.
7. R. A. Page, J. Lankford, and S. Spooner: J. Mat. Sci., 1984, vol. 19, pp. 3360-3374.
8. R. A. Page, J. Lankford, and S. Spooner: Acta Metall., 1984, vol. 32, pp. 1275-1286.
9. J. Lankford, K. S. Chan, and R. A. Page: Fracture Mechanics of Ceramics, R. C. Bradt, A. G. Evans, D. P. H. Hasselman, and F. F. Lange, eds., Plenum Press, New York (in press).
10. R. A. Page, J. Lankford, K. S. Chan, K. Hardman-Rhyne, and S. Spooner: J. Am. Ceram. Soc., (in press).
11. M. V. Speight and W. Beere: Met. Sci., 1975, vol. 9, pp. 190-191.
12. R. Raj and C. H. Dang: Phil. Mag., 1975, vol. 32, pp. 909-922.
13. K. S. Chan, J. Lankford, and R. A. Page: Acta Metall., 1984, vol. 32, pp. 1907-1914.

14. K. S. Chan, R. A. Page, and J. Lankford: Acta Metall., 1986, vol. 34, pp. 2361-2370.
15. G. W. Greenwood: Phil. Mag., 1969, vol. 19, pp. 423-427.
16. A. Gittens: Met. Sci. J., 1967, vol. 1, pp. 214-216.
17. I.-W. Chen and A. S. Argon: Acta Metall., 1981, vol. 29, pp. 1321-1333.
18. M. D. Thouless and A. G. Evans: J. Am. Ceram. Soc., 1984, vol. 67, pp. 721-727.
19. R. Raj: Acta Metall., 1978, vol. 26, pp. 995-1006.
20. A. S. Argon, I.-W. Chen, and C. W. Lau: Creep-Fatigue-Environment Interactions, R. M. Pelloux and N. S. Stoloff, eds., The Metallurgical Society of A.I.M.E., New York, 1980, pp. 46-85.
21. M. H. Yoo and H. Trinkaus: Metall. Trans., 1983, vol. 14A, pp. 547-561.
22. A. J. Perry: J. Mat. Sci., 1974, vol. 9, pp. 1016-1039.
23. W. D. Nix: Scripta Metall., 1983, vol. 17, pp. 1-4.
24. A. S. Argon: Scripta Metall., 1983, vol. 17, pp. 5-12.
25. S. H. Goods and T. G. Nieh: Scripta Metall., 1983, vol. 17, pp. 23-30.
26. B. F. Dyson: Scripta Metall., 1983, vol. 17, pp. 31-37.
27. C. B. Carter, D. L. Kohlstedt, and S. L. Sass: J. Am. Ceram. Soc., 1980, vol. 63, pp. 623-627.
28. S. C. Hansen and D. S. Phillips: Phil. Mag., 1983, vol. 47, pp. 209-234.
29. K. J. Morrissey and C. B. Carter: J. Am. Ceram. Soc., 1984, vol. 67, pp. 292-301.

30. S. M. Wiederhorn, B. J. Hockey, R. F. Krause, Jr., and K. Jakus: J. Mat. Sci., 1986, vol. 21, pp. 810-824.
31. A. G. Evans and A. S. Rana: Acta Metall., 1980, vol. 28, pp. 129-141.
32. J. R. Porter, W. Blumenthal, and A. G. Evans: Acta Metall., 1981, vol. 29, pp. 1899-1906.
33. C. S. Hsueh and A. G. Evans: Acta Metall., 1981, vol. 29, pp. 1907-1917.
34. N. G. Needlam and T. Gladman: Met. Sci. J., 1980, vol. 14, pp. 64-72.
35. I.-W. Chen and A. S. Argon: Creep and Fracture of Engineering Materials and Structures, B. Wilshire and D. R. J. Owen, eds., Pineridge Press, Swansea, U.K., 1981, pp. 289-302.
36. R. Raj: Metall. Trans., 1975, vol. 6A, pp. 1499-1509.
37. R. Raj and M. F. Ashby: Metall. Trans., 1971, vol. 2, pp. 1113-1127.
38. A. G. Evans, J. R. Rice, and J. P. Hirth: J. Am. Ceram. Soc., 1980, vol. 63, pp. 368-375.
39. H. Hubner and J. Stark: Proceedings of the 6th CIMTEC, Milan, Italy, 1986, in press.
40. A. G. Evans and T. G. Langdon: Progress in Materials Science, 1976, vol. 21, No. 3/4, pp. 396-399.
41. H. Gleiter and B. Chalmers: Progress in Materials Science, 1971, vol. 16, pp. 181-207.
42. B. F. Dyson: Met. Sci. J., 1976, vol. 10, pp. 349-353.

43. J. Intrater and E. Machlin: *J. Inst. Metals*, 1959-60, vol. 88, pp. 305-310.
44. F. N. Rhines, W. E. Bond, and M. A. Kissel: *Trans. ASM*, 1956, vol. 48, pp. 919-951.
45. S. K. Tung and R. Maddin: *Trans. AIME*, 1957, vol. 209, pp. 905-910.
46. F. Weinberg: *Acta Met.*, 1954, vol. 2, pp. 889-890.
47. F. Weinberg: *Trans. AIME*, 1958, vol. 212, pp. 808-817.
48. K. E. Putlick and R. King: *J. Inst. Met.*, 1951-52, vol. 80, pp. 537-544.
49. H. Gleiter and B. Chalmers: High-Angle Grain Boundaries, *Progress in Mat. Sciences*, vol. 16, Pergamon Press, Oxford, 1972, Ch. 7, pp. 179-217.
50. H. J. Larson and B. O. Shubert: Probabilistic Models in Engineering Sciences, Wiley, New York, vol. 2, 1979, Ch. 7, pp. 544-583.
51. S. J. Fairborz, D. G. Harlow, and T. J. Delph: Acta Metall., 1986, vol. 34, pp. 1433-1441.
52. K. S. Chan and R. A. Page: Southwest Research Institute, San Antonio, TX, unpublished research, 1987.
53. J. S. Wang, J. J. Stephens, and W. D. Nix: *Acta Met.*, 1985, vol. 33, pp. 1009-1021.
54. I.-W. Chen: Metall. Trans., 1983, vol. 14A, pp. 2289-2293.
55. K. S. Yu and W. D. Nix: Scripta Metall., 1984, vol. 18, pp. 173-178.
56. A. W. Mullendore and N. J. Grant: Trans. AIME, 1963, vol. 227, pp. 319-330.

57. B. Fazan, O. D. Sherby, and J. E. Dorn: Trans. AIME, 1954, vol. 200, pp. 919-922.
58. W. Beere and G. K. Knowles: Scripta Metall., 1982, vol. 16, pp. 23-28.
59. J. Lankford: Southwest Research Institute, San Antonio, TX, private communication, 1986.
60. W. Weibull: J. of App. Mech., 1951, vol. 18, pp. 293-297.
61. F. A. McClintock: Fracture Mechanics of Ceramics, R. C. Bradt, D. P. H. Hasselman, and F. F. Lange, eds., Plenum Press, New York, vol. 1, 1974, pp. 93-101.
62. R. L. Orr, O. D. Sherby, and J. E. Dorn: Trans. ASM, 1954, vol. 46, pp. 113-128.
63. S. J. Fairborz, D. G. Harlow, and T. J. Delph: Acta Metall., 1985, vol. 33, pp. 1-9.

## LIST OF FIGURE CAPTIONS

- Figure 1. Number of cavities per unit volume versus time for a hot-pressed silicon carbide, NC203, and two sintered aluminas, AD99 and Lucalox. Both the hot-pressed silicon carbide and the AD99 alumina contained a continuous, glassy grain boundary phase. The Lucalox alumina contained glass free grain boundaries.
- Figure 2. Schematic of an inclined, faceted grain boundary (ABCD) with a ledge (BC) subject to a remote compressive stress,  $\sigma_{\infty}$ , and the inducement of local tensile stresses at the ledge by the sliding of boundary segments AB and CD.
- Figure 3. The stress concentration factor at the center of an 8 nm high ledge as a function of time,  $t$ , normalized by the characteristic time for grain boundary diffusion,  $t_c$ .
- Figure 4. Comparison of two estimates of the incubation time for cavity nucleation,  $t_i^u$  and  $t_i^l$ , with the characteristic times for relaxing stress concentration at a 10 nm high GB ledge by either grain boundary diffusion,  $t_c$ , or power-law creep,  $t_p$ . Also indicated is  $t_{BR}$ , the characteristic time for relaxing the shear stresses along sliding grain boundaries. The range of  $h/\lambda$  at which  $t_c \geq t_i \geq t_{BR}$  occurs is  $\sim 1-3 \times 10^{-2}$ .

- Figure 5. Stress concentration factor at an 8 nm high grain boundary ledge as a function of the ledge height to spacing ratio,  $h/\lambda$ . The stress concentration factor is evaluated at  $x = 0$  and  $t = t_i$  for equilibrium-shaped cavities with  $F_V = 1.24$ ;  $t_i$  is the incubation time for cavity nucleation.
- Figure 6. Increase in individual cavity radius with time. Time denotes the elapsed time since cavity nucleation and  $r_c$  is the critical cavity radius.
- Figure 7. A schematic of a cavitating grain boundary, BE, subject to a remotely applied compressive load illustrating the development of tensile stresses on the cavitating boundary as the result of sliding on adjacent boundaries.
- Figure 8. Comparison of calculated and measured volume of an individual cavity as a function of time. Both the experimental and theoretical curves are for AD99 alumina crept at 1150°C and 220 MPa, as described in Ref. (10).
- Figure 9. A schematic showing the probability density function of grains sliding at a given value of  $\lambda$  changes with time as the result of stochastic grain boundary sliding. Note that  $\lambda = 1$  for grains which deform by grain boundary sliding only, and  $\lambda = 0$  for grains which deform by creep only. The majority of the grains deform by both creep and grain boundary sliding.

Figure 10. Schematics showing the dependence of  $\mu'(t)$ ,  $N_V/V$ ,  $\lambda'(t)$ , and  $\dot{n}$  on the range of  $m$  values admissible in a Poisson process.

Figure 11. Formation of a facet-sized cavity by nucleation of cavities at grain boundary ledges and the growth and coalescence of these cavities: (a) in a ceramic without a glassy phase along the grain boundary, and (b) in a ceramic with a glassy phase along the grain boundary.

Figure 12. Formation of a facet-sized cavity for continuous nucleation of cavities which show no apparent growth after reaching a critical size: (a) in a ceramic without a glassy phase along the grain boundary, and (b) in a ceramic with a glassy phase along the grain boundary.

Figure 13. Coalescence of facet-sized cavities in ceramics: (a) ceramics under tension (after Evans and Rana<sup>31</sup>); (b) ceramics under compression (after Lankford<sup>43</sup>).

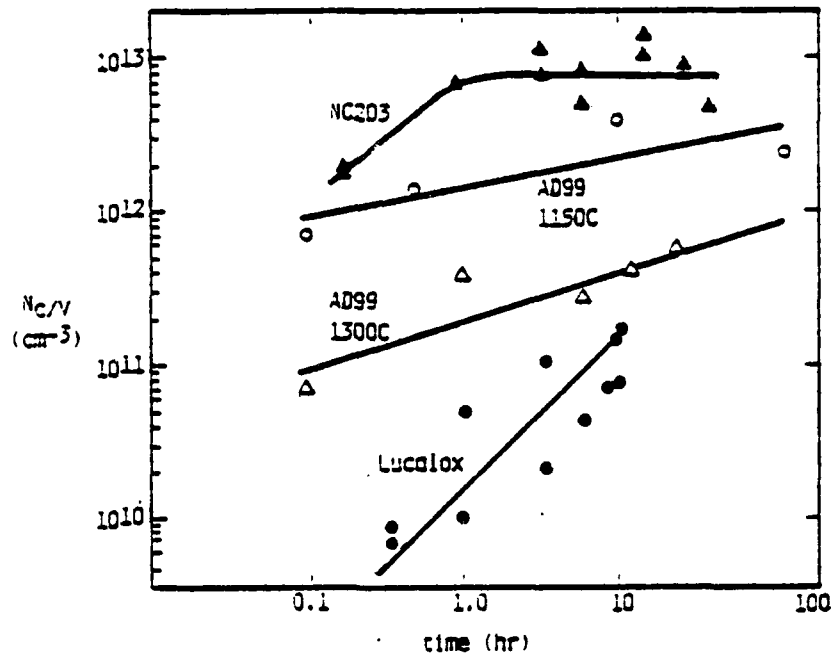
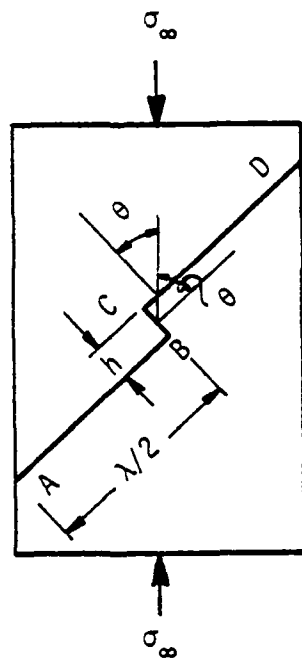
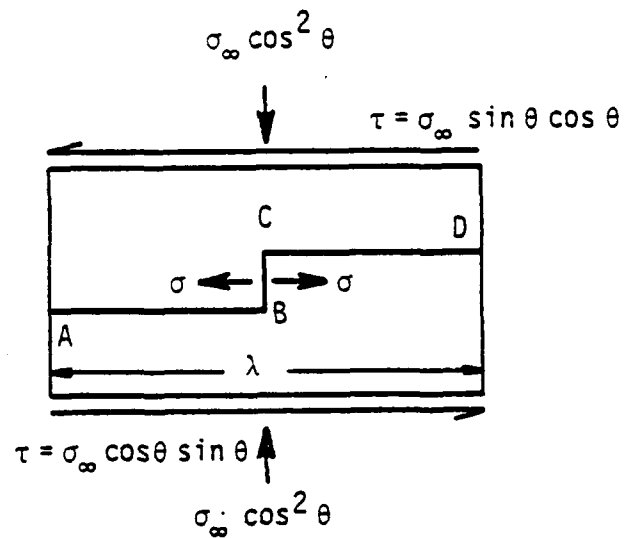


Fig. 1. Number of cavities per unit volume versus time for a hot-pressed silicon carbide, NC203, and two sintered aluminas, AD99 and Lucalox. Both the hot-pressed silicon carbide and the AD99 alumina contained a continuous, glassy grain boundary phase. The Lucalox alumina contained glass free grain boundaries.



(a)



(b)

Fig. 2. Schematic of an inclined, faceted grain boundary (ABCD) with a ledge (BC) subject to a remote compressive stress,  $\sigma_\infty$ , and the inducement of local tensile stresses at the ledge by the sliding of boundary segments AB and CD.

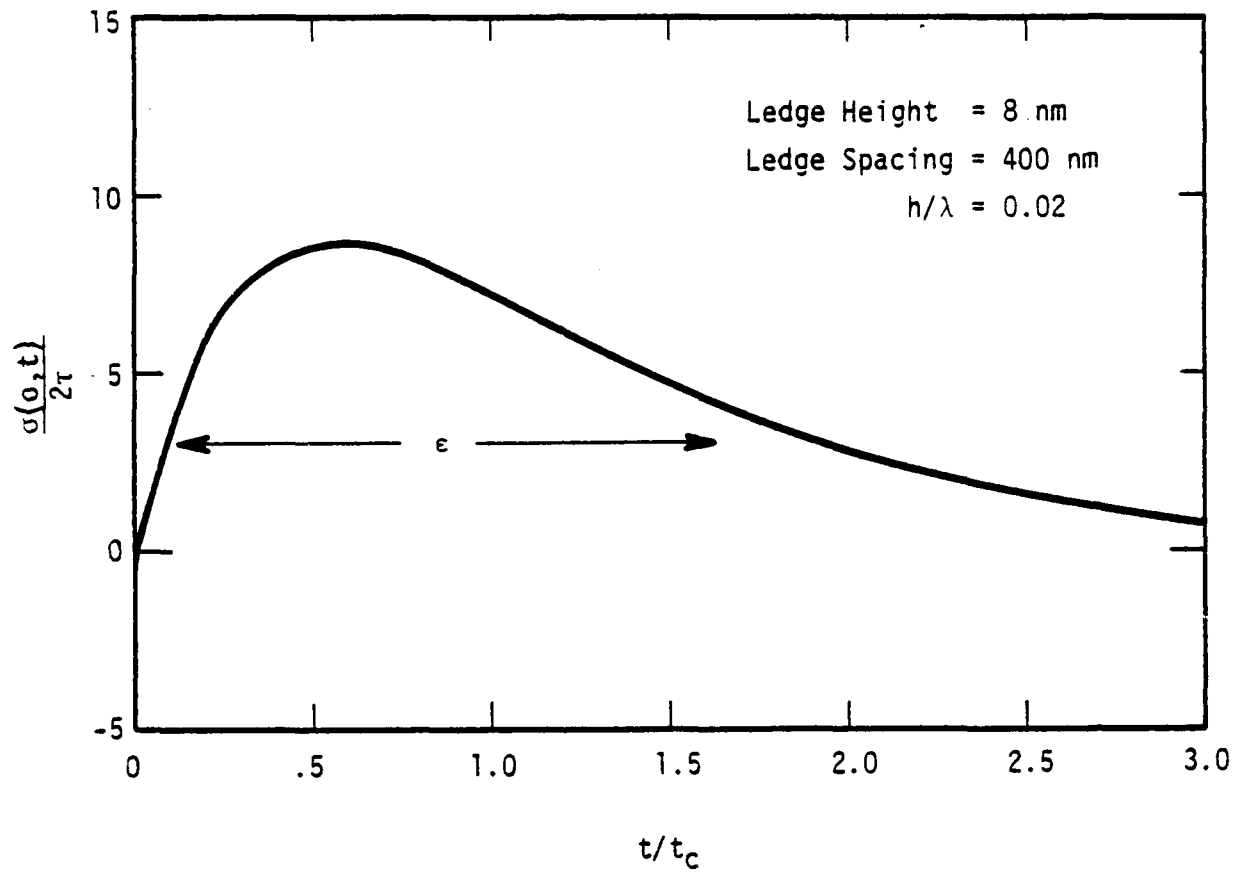


Fig. 3. The stress concentration factor at the center of an 8 nm high ledge as a function of time,  $t$ , normalized by the characteristic time for grain boundary diffusion,  $t_c$ .

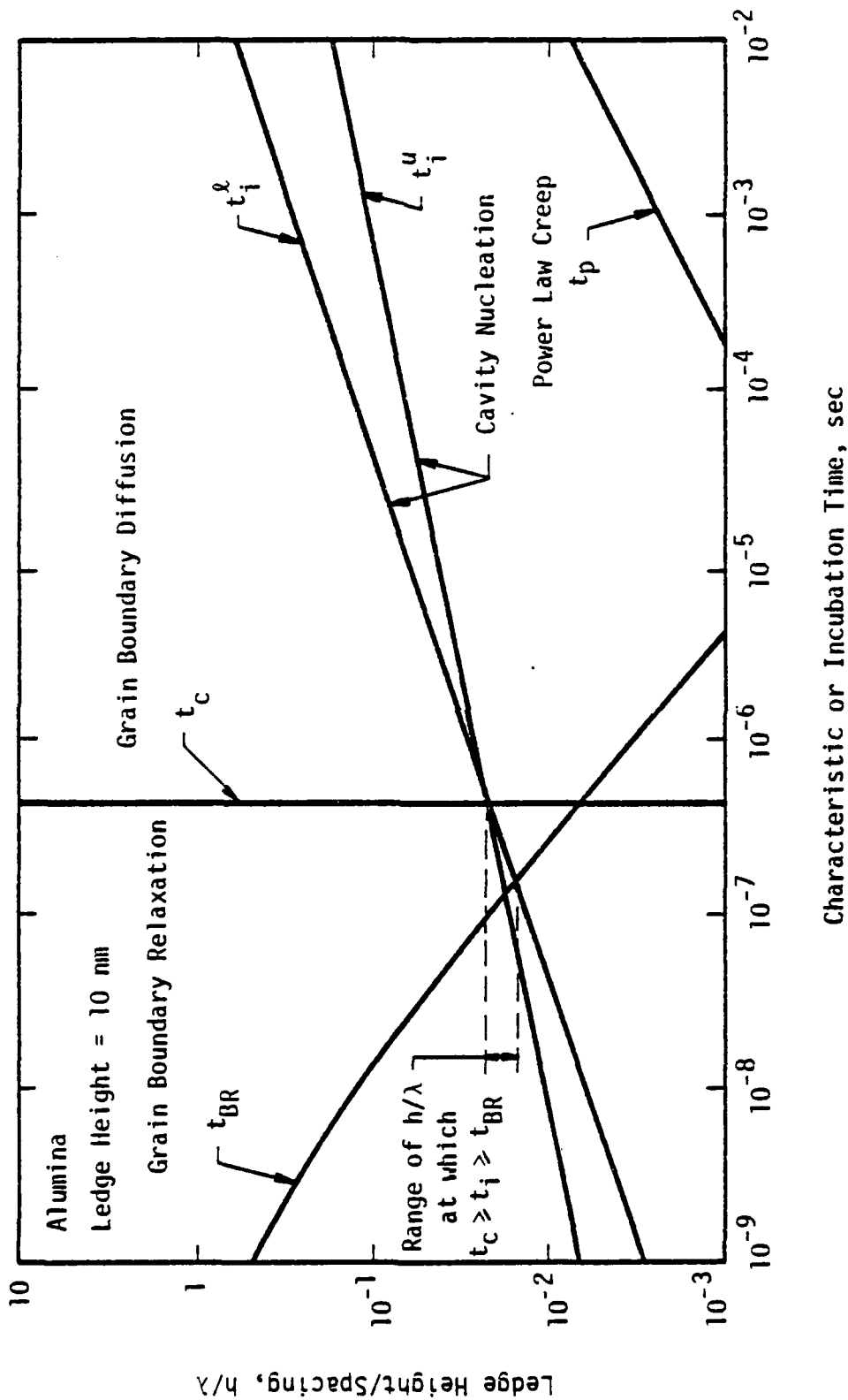


Fig. 4. Comparison of two estimates of the incubation time for cavity nucleation,  $t_i^u$  and  $t_i^l$ , with the characteristic times for relaxing stress concentration at a 10 nm high GB ledge by either grain boundary diffusion,  $t_c$ , or power-law creep,  $t_p$ . Also indicated is  $t_{BR}$ , the characteristic time for relaxing the shear stresses along sliding grain boundaries. The range of  $h/\lambda$  at which  $t_c \geq t_i \geq t_{BR}$  occurs is  $\sim 1-3 \times 10^{-2}$ .

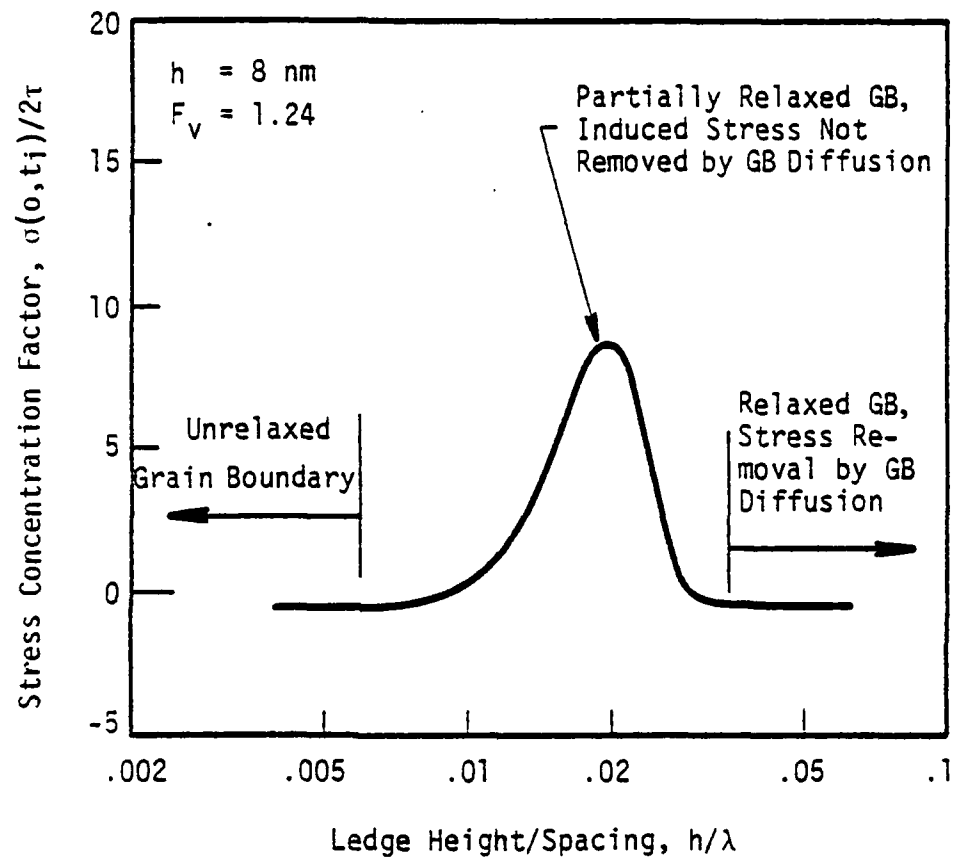


Fig. 5. Stress concentration factor at an 8 nm high grain boundary ledge as a function of the ledge height to spacing ratio,  $h/\lambda$ . The stress concentration factor is evaluated at  $x = 0$  and  $t = t_i$  for equilibrium-shaped cavities with  $F_v = 1.24$ ;  $t_i$  is the incubation time for cavity nucleation.

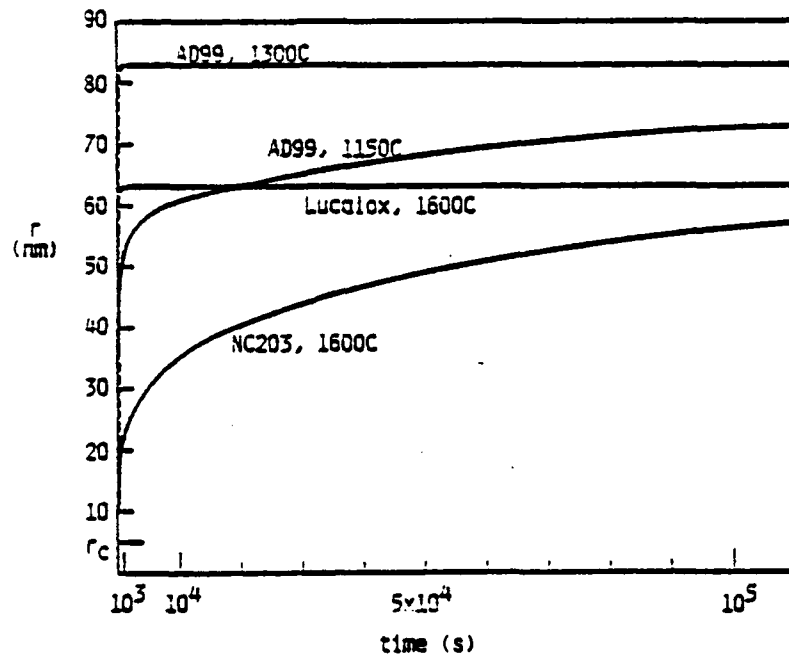


Fig. 6. Increase in individual cavity radius with time. Time denotes the elapsed time since cavity nucleation and  $r_c$  is the critical cavity radius.

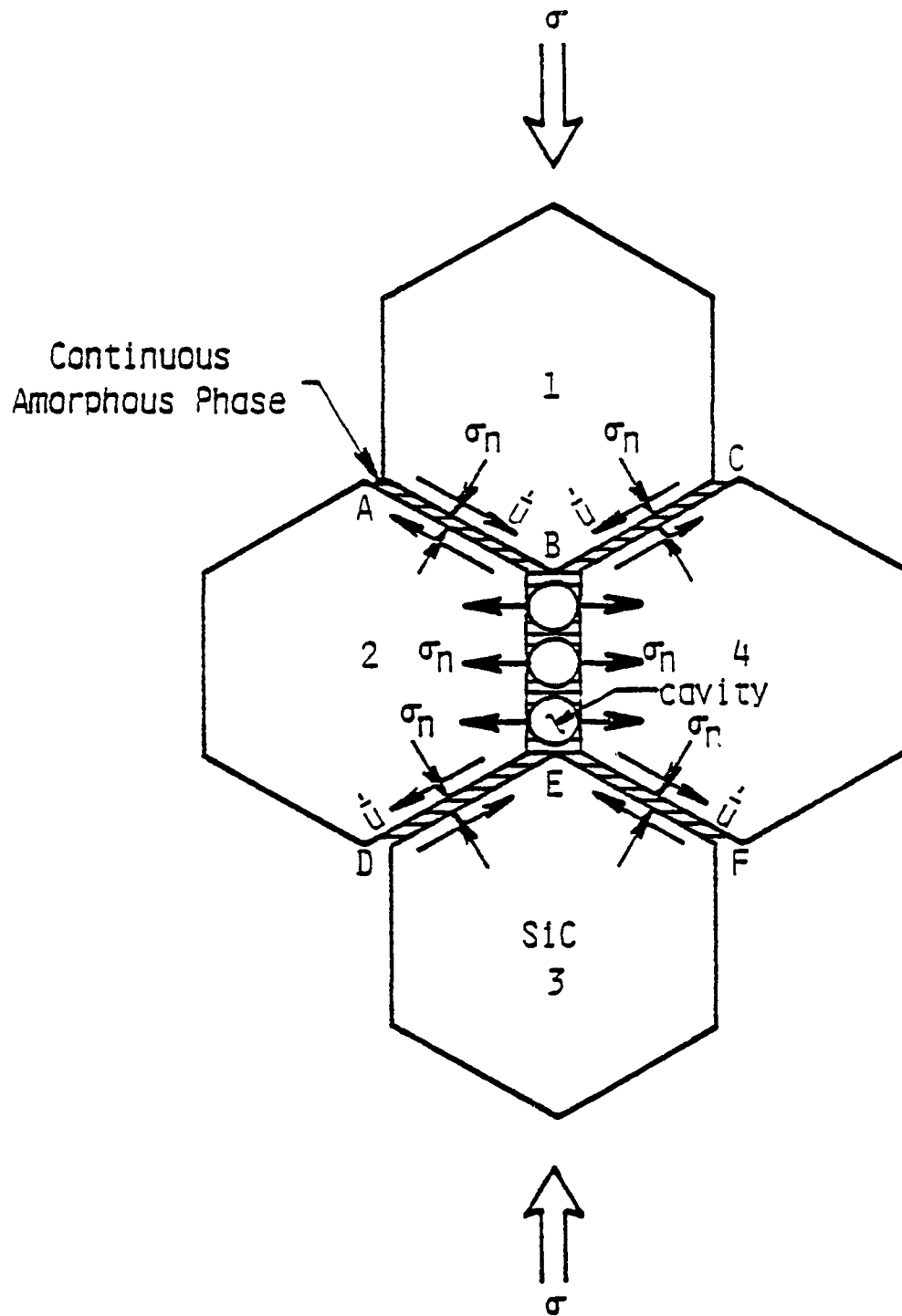


Fig. 7. A schematic of a cavitating grain boundary, BE, subject to a remotely applied compressive load illustrating the development of tensile stresses on the cavitating boundary as the result of sliding on adjacent boundaries.

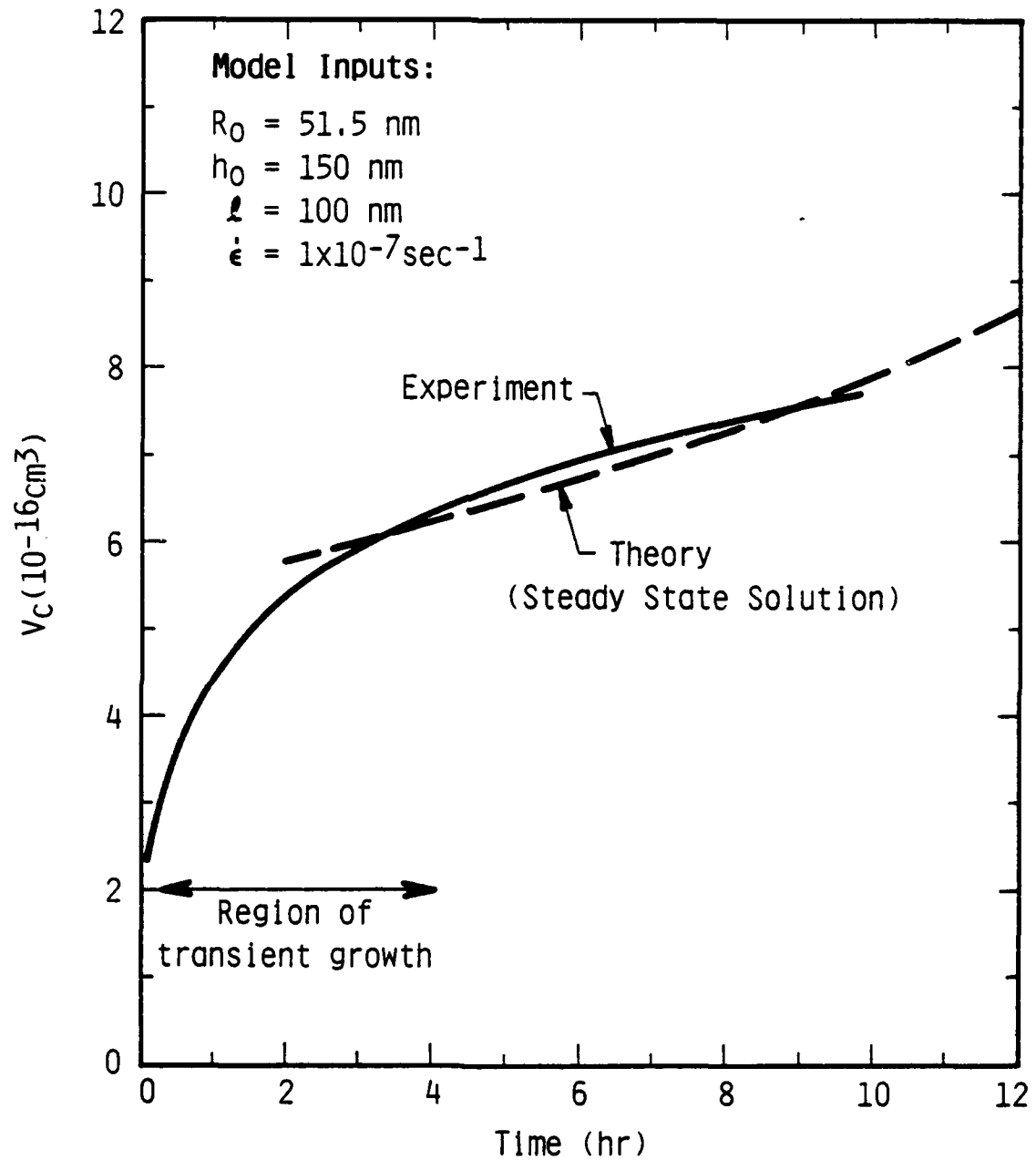


Fig. 8. Comparison of calculated and measured volume of an individual cavity as a function of time. Both the experimental and theoretical curves are for AD99 alumina crept at 1150°C and 220 MPa, as described in Ref. (10).

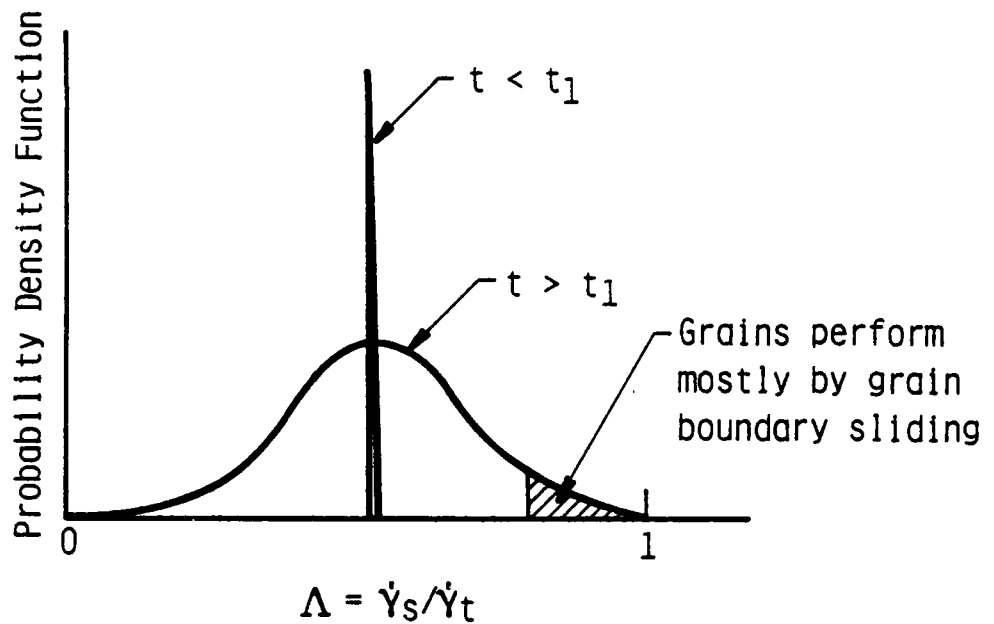


Fig. 9. A schematic showing the probability density function of grains sliding at a given value of  $\Lambda$  changes with time as the result of stochastic grain boundary sliding. Note that  $\Lambda = 1$  for grains which deform by grain boundary sliding only, and  $\Lambda = 0$  for grains which deform by creep only. The majority of the grains deform by both creep and grain boundary sliding.

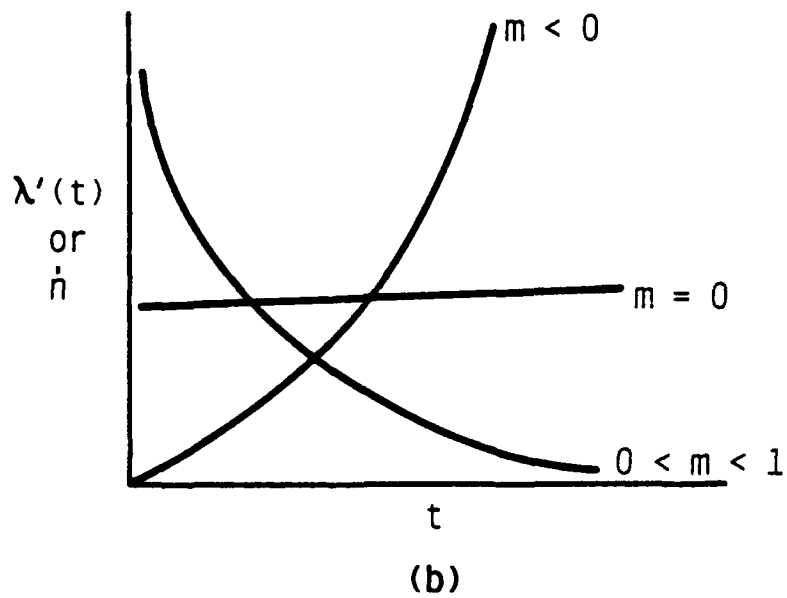
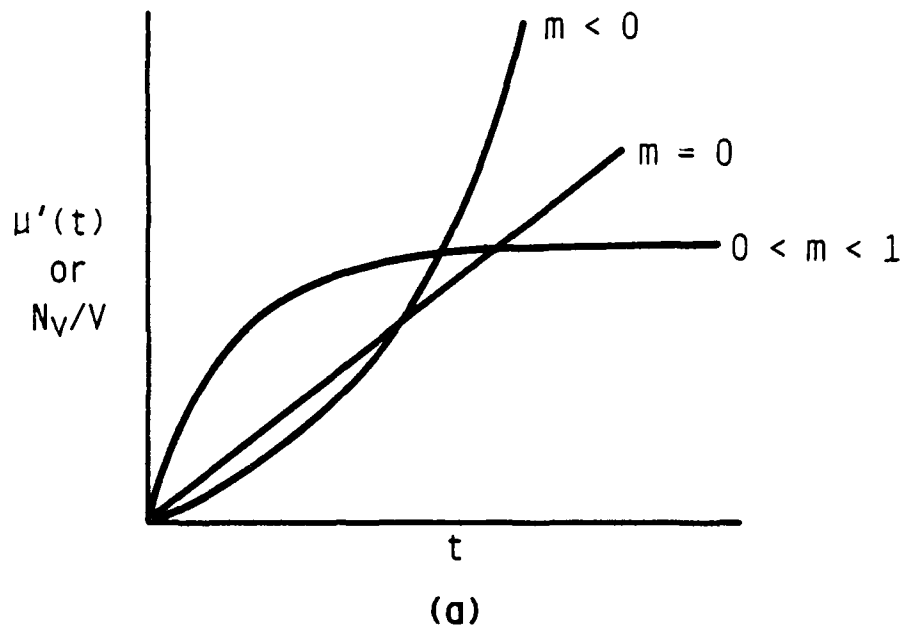


Fig. 10. Schematics showing the dependence of  $\mu'(t)$ ,  $N_V/V$ ,  $\lambda'(t)$ , and  $\dot{n}$  on the range of  $m$  values admissible in a Poisson process.

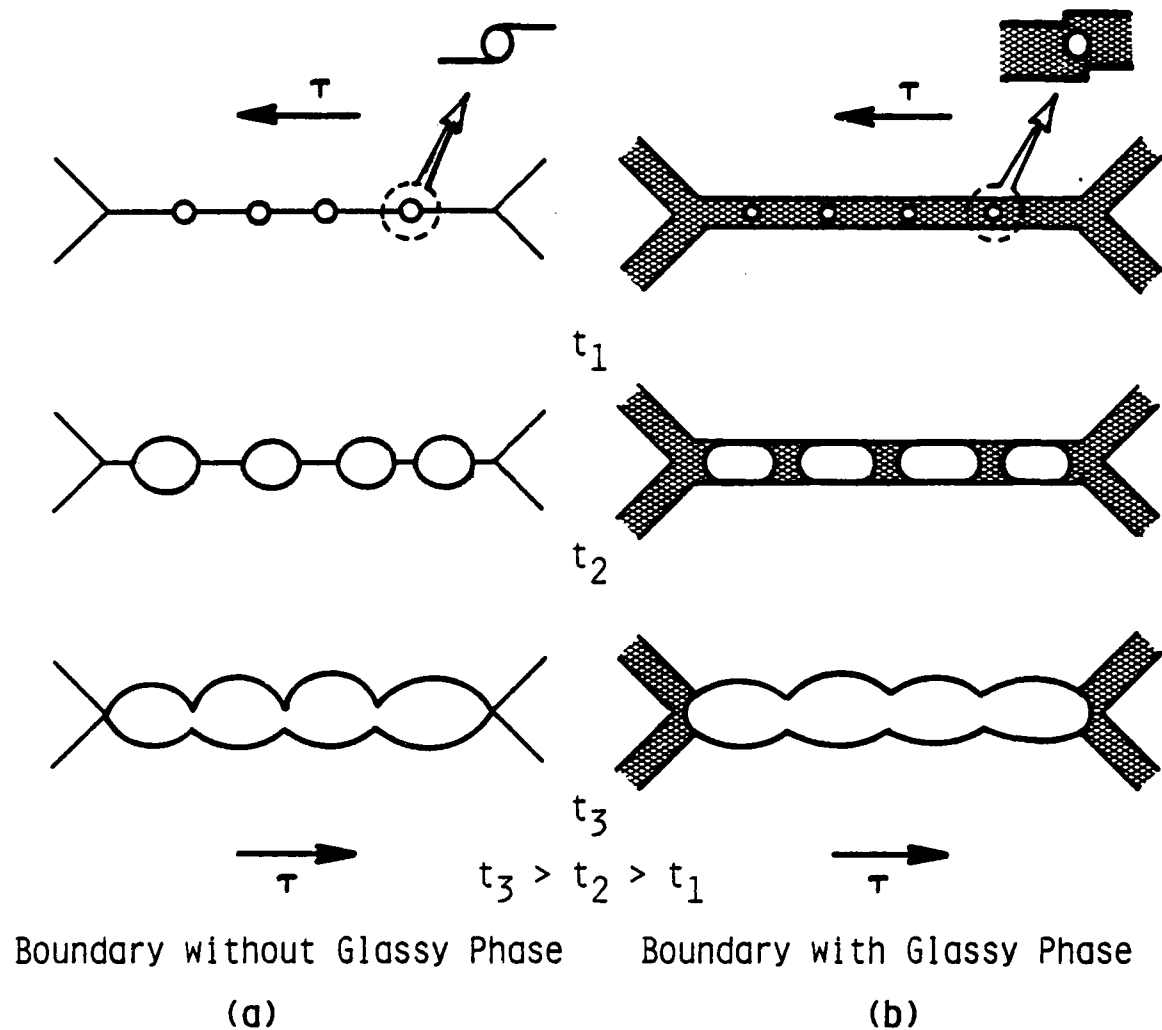


Fig. 11. Formation of a facet-sized cavity by nucleation of cavities at grain boundary ledges and the growth and coalescence of these cavities: (a) in a ceramic without a glassy phase along the grain boundary, and (b) in a ceramic with a glassy phase along the grain boundary.

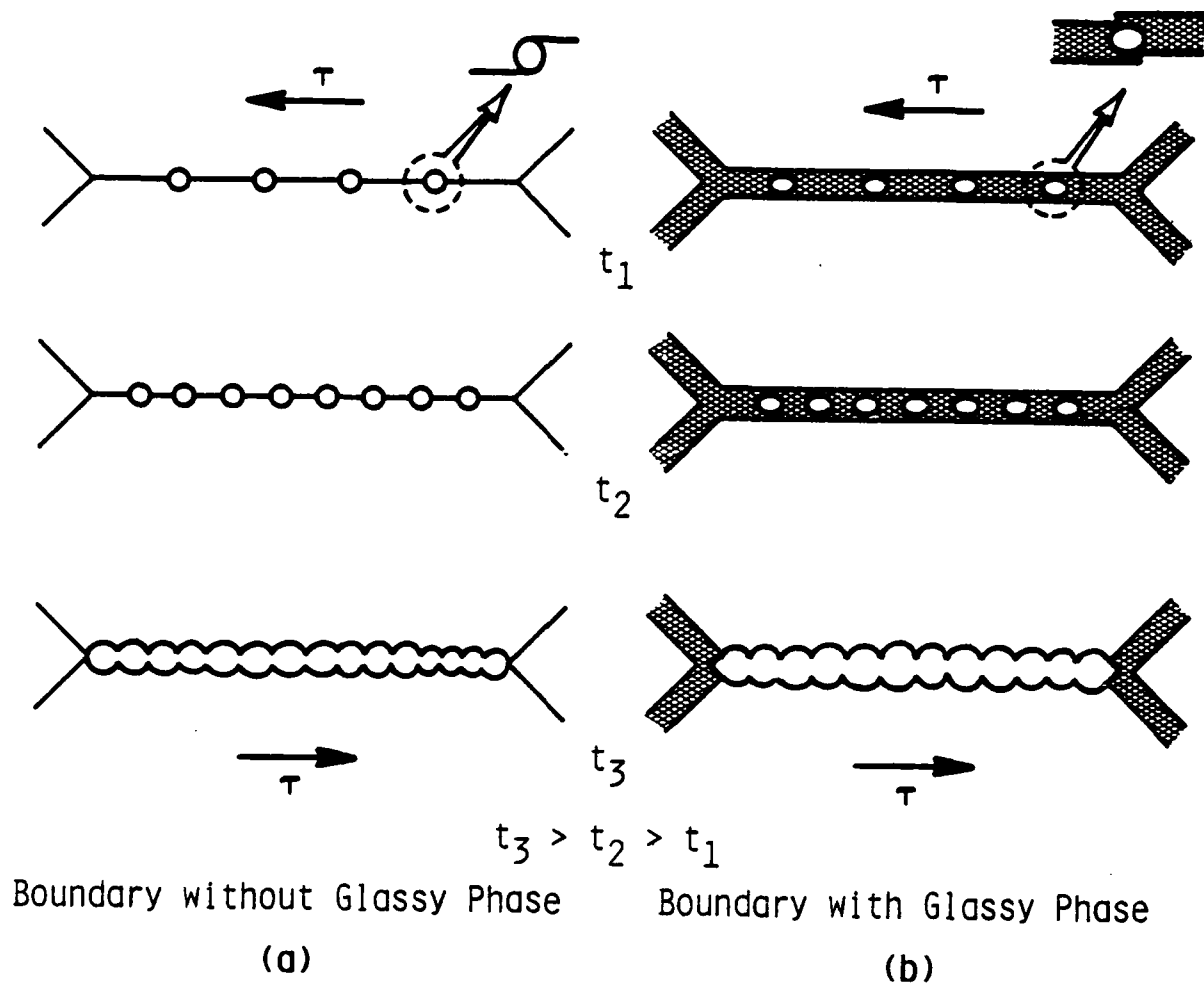


Fig. 12. Formation of a facet-sized cavity for continuous nucleation of cavities which show no apparent growth after reaching a critical size: (a) in a ceramic without a glassy phase along the grain boundary, and (b) in a ceramic with a glassy phase along the grain boundary.

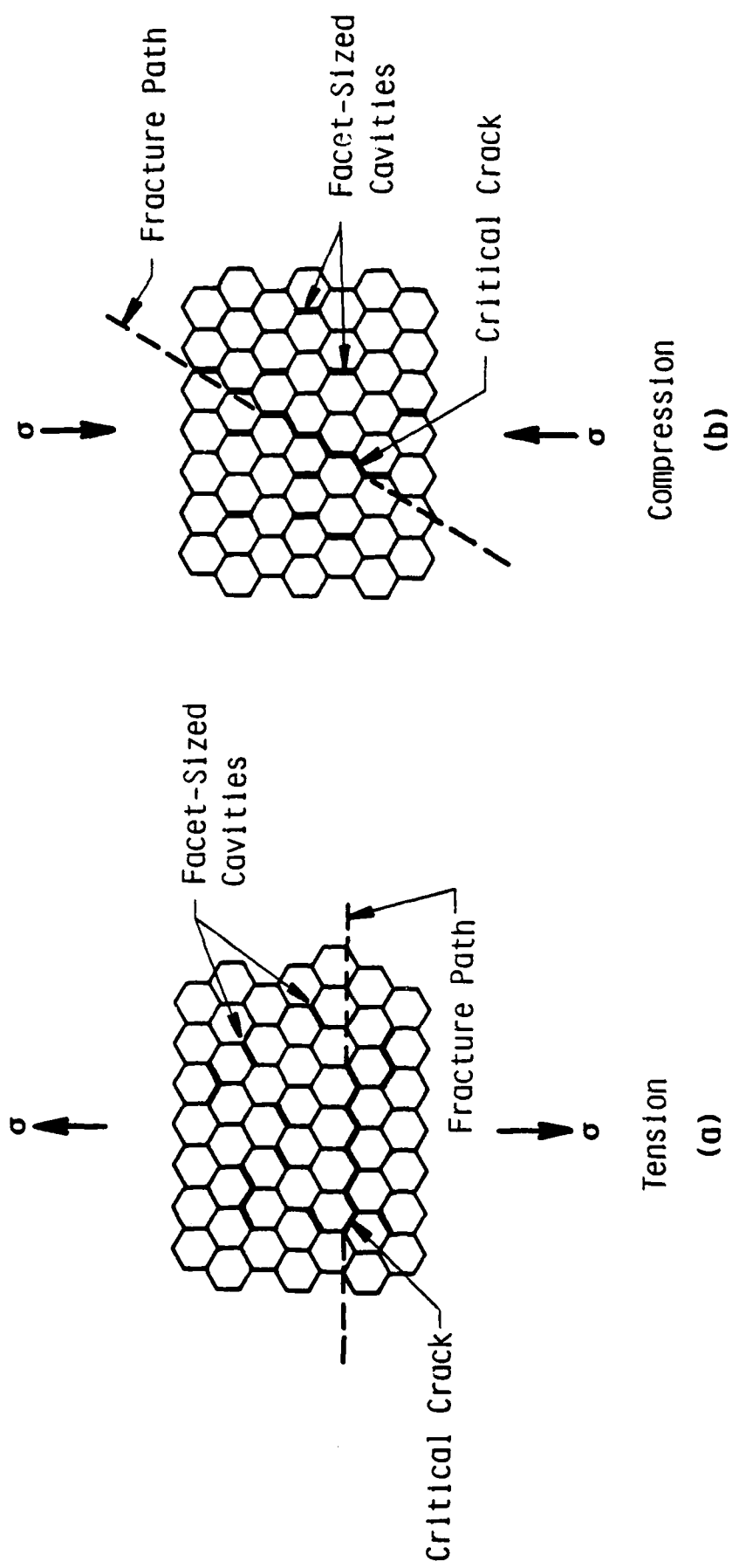


Fig. 13. Coalescence of facet-sized cavities in ceramics: (a) ceramics under tension (after Evans and Rana<sup>31</sup>); (b) ceramics under compression (after Lankford<sup>43</sup>).